Interdecadal Variability of the Thermohaline Circulation in Box-Ocean Models Forced by Fixed Surface Fluxes

THIERRY HUCK AND ALAIN COLIN DE VERDIÈRE

Laboratoire de Physique des Océans, Université de Bretagne Occidentale, Brest, France

ANDREW J. WEAVER

School of Earth and Ocean Sciences, University of Victoria, Victoria, British Columbia, Canada

(Manuscript received 1 July 1997, in final form 28 May 1998)

ABSTRACT

Intrinsic modes of decadal variability are analyzed using box-geometry ocean models forced by constant surface fluxes. An extensive parameter sensitivity analysis of the oscillatory behavior is carried out with respect to the spherical/Cartesian geometry, the β effect, the Coriolis parameter, the parameterization of momentum dissipation and associated boundary conditions, the vertical and horizontal diffusivities, the convective adjustment algorithm, the horizontal and vertical model resolution, the forcing amplitude, and the basin width. The oscillations stand out as a robust geostrophic feature whose amplitude is mainly controlled by the horizontal diffusivity. Unsuccessful attempts to reproduce the variability in zonally averaged 2D models suggest that the 3D adjustment processes are necessary. However, the β effect is not necessary for decadal variability to occur, and therefore classical Rossby waves play no fundamental role in the mechanism. Various experiments with different geometry and forcing are conducted and do not support the necessity of viscous numerical boundary waves or any boundary in sustaining the oscillations. The models show two types of oscillatory behavior: 1) temperature anomalies propagating geostrophically westward in the eastward jet (northern part of the basin) and inducing an opposite anomaly in their wake and 2) stationary temperature anomalies in the northwest quarter that respond to the western boundary current transport changes and reinforce geostrophically this change until the opposite temperature anomaly built on the east finally reverses the meridional overturning anomaly. The analysis of the transition from steady to oscillatory states (using heat fluxes diagnosed at the equilibrium under restoring boundary conditions) and the comparison of the variability under various forcing fields suggest that the oscillations are triggered in the regions of strongest surface cooling. Finally, a simple box-model analogy is proposed that captures the crucial phase shift between meridional overturning and north–south density gradient anomalies on these decadal timescales.

1. Introduction

Analysis of hydrographic and other data has recently revealed that the coupled ocean–atmosphere system is variable on decadal timescales (Deser and Blackmon 1993; Kushnir 1994; Hansen and Bezdek 1996; Reverdin et al. 1997). This has important ramifications for global climate change since before one can unambiguously detect a signal of anthropogenic global warming, one must acquire an understanding of the free modes of variability of the climatic system. Furthermore, the analysis of the present state of the coupled system in terms of these modes reveals the potential for some predictability on a few years (Griffies and Bryan 1997). Coupled atmosphere–ocean models appear to be able to reproduce observed patterns of interdecadal variability involving the thermohaline circulation (Delworth et al. 1993). However, a dynamical atmospheric component does not seem necessary to reproduce this variability since Greatbatch and Zhang (1995, GZ95 hereafter) found very similar oscillations in an idealized ocean basin forced by constant heat fluxes. The relatively long timescale of interdecadal oscillations compared to atmospheric thermal inertial timescales suggests such a fundamental oceanic contribution. On the other hand, decadal oscillations have been described previously in ocean models forced with mixed boundary conditions (Weaver and Sarachik 1991). Such boundary conditions since have been shown to lead to idiosyncratic behaviors (Zhang et al. 1993) and do not represent properly the large-scale atmosphere–ocean interactions (e.g., see Capotondi and Saravanan 1996). Consequently, we analyze further the variability in noncoupled ocean models forced by fixed surface fluxes.

Numerous ocean models forced by constant flux

Corresponding author address: Thierry Huck, GFDL, Princeton University, Forrestal Campus Route 1, Princeton, NJ 08542.
E-mail: tnh@gfdl.gov

© 1999 American Meteorological Society

boundary conditions were found to generate purely oceanic decadal-scale variability (Huang and Chou 1994, hereafter HC94; Chen and Ghil 1995; GZ95; Winton 1996, hereafter W96; Greatbatch and Peterson 1996, hereafter GP96). Even a zonally averaged ocean model coupled to a two-level atmospheric model exhibited variability on interdecadal timescales (Saravanan and McWilliams 1995). Since W96 reported no oscillation in a zonally averaged ocean model forced by constant surface heat fluxes (although the same fluxes induce decadal oscillations when applied to a fully three-dimensional model), we conclude that it is the synoptic variability of the atmospheric component that sustains the oceanic variability in the Saravanan and McWilliams model. Further, we consider only constant oceanic surface forcing.

Winton (1996) reproduced the decadal oscillation found in ocean general circulation models on an f plane, thus discarding the β effect from the driving mechanisms and classical Rossby waves for setting the decadal period. Nevertheless, we will show that the variability patterns are quite different on f and β planes. GP96, in agreement with W96, proposed an explanation based on the propagation of frictional boundary waves (the viscous analog of Kelvin waves when no time derivative is retained in the momentum equation). They suggested that these waves are sufficiently slowed along the weakly stratified polar boundaries, where convection takes place, to give rise to decadal periods. We do not find any evidence for this mechanism in our simulations. Furthermore, it does not provide a source of energy for sustaining the oscillations against dissipation. Our aim in this paper is therefore to analyze further the variability in box-ocean models forced by constant fluxes and to determine the physical processes driving the nonsteadiness of the thermohaline circulation and modulating it in interdecadal timescales. We focus on the purely thermally forced ocean circulation for simplicity, and in order to get the essence of the variability, the wind stress is set to zero in all the experiments (except in section 6).

Most of the numerical experiments that we perform are based on the planetary geostrophic equations, but direct comparisons with the Geophysical Fluid Dynamics Laboratory Modular Ocean Model (GFDL MOM) support our choice of equations for the relatively coarse resolution used (160 km) on a midlatitude ocean domain. For each experiment, we use the same geometry, parameters, and forcing but allow for different parameterizations of momentum dissipation and associated boundary conditions in order to discard any conclusions that would be specific to one model. We show that decadal oscillations appear spontaneously under zonally uniform constant heat flux (varying with latitude) in a large realistic range of parameters. More appropriate westerly intensified fluxes, diagnosed at the equilibrium under restoring boundary conditions, also produce these oscillations. In order to identify the mechanism exciting the variability, we carry out an extensive parameter sensitivity study, similar to the work of HC94 for the haline circulation. After discarding convection and the β effect from the processes necessary for the variability to occur, we show that the oscillations appear to be primarily geostrophically driven, but very sensitive to the damping by horizontal diffusion, and more likely to be generated by a strong circulation. The role of the boundaries is then analyzed: in comparison with GP96, we extend the ocean basins with buffer regions where no forcing is applied, successively in each of four directions. The western boundary current is finally removed by making the domain periodic in the east–west direction. Additional experiments with a forcing symmetric in latitude (that eliminates the weakly stratified boundary) suggest that a boundary wave propagation mechanism is not always appropriate. Then, we try to determine the origin of the variability in the analysis of the transient phase from a steady circulation to a regular oscillatory behavior when restoring boundary conditions are changed into diagnosed fixed fluxes. The initial perturbations appear in the regions of strongest surface cooling and the amplification of the anomalies in the vicinity of the western boundary is geostrophically driven. Finally, we propose a simple box model formulation that captures the phase shift between the strength of the meridional cell and the north–south density gradient anomalies.

The rest of the paper is organized as follows: section 2 briefly describes the models used, section 3 reports on the parameter sensitivity analysis, and section 4 looks at the role of the boundaries. Section 5 provides hints to the variability mechanism through the transition from restoring to fixed flux boundary conditions. The robustness of the variability to various parameterizations and processes is discussed in section 6 and conclusions are given in section 7.

2. The models

The models we use are described in detail in Huck et al. (1999, HWC hereafter) and Huck (1997). They are based on the Cartesian coordinate planetary geostrophic equations (Phillips 1963; Hasselmann 1982; Salmon 1986, 1990; Colin de Verdière 1988, 1989; Zhang et al. 1992; Winton 1993) and rely on the hydrostatic and Boussinesq approximations. A version of these models is also developed in spherical coordinates to assess the validity of our Cartesian coordinates assumption. The GFDL MOM (Pacanowski 1995), based on the primitive equations, is used to validate the planetary geostrophic assumption (see also HWC). The geometry is not modified from HWC: a flat-bottomed β-plane ocean domain centered at 40°N, extending from 20°N to 60°N, 5120 km wide and 4500 m deep. The resolution is similar in most of the experiments: 160 km horizontally, 15 levels vertically (respectively, 50×3, 100, 150, 200, 250, 300, 350, 400, 450, 500, 550×3 m deep). Wind stress is set to zero in order to simplify

the analysis of the purely thermohaline variability, but this does not profoundly influence the variability (see section 6). Traditional subgrid-scale Laplacian parameterizations are used for tracer diffusion (700 and 10^{-4} m^2 s^{-1}, respectively, for the horizontal and vertical diffusivities) along with the convective adjustment scheme described by Rahmstorf (1993). For momentum dissipation, no vertical viscosity is used in most cases, since the high horizontal friction needed to resolve the frictional boundary layers within our coarse grid has a much greater influence (see section 3i). Horizontal viscosity is parameterized either by the usual Laplacian operator [in the planetary geostrophic model with Laplacian friction (PGL) and GFDL MOM] with a 1.5×10^5 m^2 s^{-1} viscosity A_H to solve for the Munk western boundary layer $(A_H/\beta)^{1/3}$, given the horizontal resolution, or by a simpler linear drag [in the planetary geostrophic models with Rayleigh friction, with no-slip boundary condition or (PGR0) Winton's vorticity closure (PGRW)] with a friction coefficient ε_H set to 4.4×10^{-6} s^{-1} (6% of the rotation rate of the earth) to solve for the Stommel frictional boundary layer (ε_H/β).

Most of the models we use implement a no-slip boundary condition: the GFDL MOM, PGL (Colin de Verdière 1988; Winton 1993), PG0, and PGR0 (Zhang et al. 1992). Two models depart fundamentally from this group: implementing a no-normal-flow boundary condition, they rely on a vorticity balance for solving the tangential velocities allowed along the boundaries. Since the frictional vorticity equation incorporates the continuity equation through the stretching term (fw_Z), this closure efficiently reduces the vertical velocities along the lateral boundaries by allowing horizontal recirculation of flows impinging into coasts, profoundly influencing the whole overturning and deep water properties. Curiously, the associated models PGRW (Winton 1993; Winton and Sarachik 1993) and planetary geostrophic with a three-dimensional linear friction relaxing the hydrostatic approximation (PGS);(Salmon 1986, 1990), are the most reluctant to sustain variability, perhaps because of the weak overturning and overall velocities they produce (see section 3h).

The sensitivity tests are carried out with the same forcing: a ''linear'' fixed surface heat flux, zonally uniform and varying linearly with latitude from 45 W m^{-2} at 20°N to -45 W m^{-2} at 60°N (the area-average is then zero on the Cartesian grid). One might argue that using temperature as the only density variable with a flux boundary condition does not match with the presupposed fast relaxation of SST anomalies under real atmospheric forcing. Actually, the large spatial scale of the SST anomalies we observe here, which have therefore a significant influence on the atmospheric temperature, hence dramatically lengthens the typical radiative damping timescale (Seager et al. 1995; Rahmstorf and Willebrand 1995; Marotzke and Pierce 1997). Furthermore, GZ95 noted that in coupled models, changes in the poleward heat transport determine predominantly the local heat content in the convection regions. Mixed boundary conditions have been thoroughly used in large-scale ocean modeling during the last decades, but lead to idiosyncratic behaviors like the polar halocline catastrophe (Zhang et al. 1993). The strong thermal relaxation they imply drives the direct thermohaline cell, but does not allow for SST changes unless unrealistically large surface fluxes are induced, although on the large scale, the oceanic heat capacity is far greater than the atmosphere's. Fixed freshwater flux allows more freedom for the salinity anomalies to develop and play a leading role regarding the variability of the circulation. Thus, analyses of decadal oscillations within mixed boundary conditions have focused on the role of salinity anomalies: Weaver and Sarachik (1991), then Yin and Sarachik (1995), proposed an advective–convective mechanism involving the circulation of salinity anomalies in the subpolar gyre, for instance. Nevertheless, it has been shown that mixed boundary conditions produce unrealistic feedbacks (Zhang et al. 1993; Power and Kleeman 1994), therefore we use instead constant fluxes, a good first-order approximation as suggested by Chen and Ghil (1996) from the coupling of an ocean model with an atmospheric energy balance model. Here, temperature only is used as a simple and meaningful way to deal with density: the heat forcing should be considered as a global buoyancy one. We then study the thermal direct cell and the role of density advection feedbacks within its circulation.

As reported by GZ95 and HC94, respectively, for the thermally and salinity driven circulations, zonally uniform buoyancy fluxes (varying with latitude) can induce decadal oscillations. Cai et al. (1995) added that a small zonal redistribution of surface buoyancy fluxes diagnosed at equilibrium under restoring boundary condition triggers interdecadal variability. In fact, in most of our models, we observe that zonal redistribution is not required, in agreement with GP96. For some of the experiments described in HWC, the shift from restoring boundary conditions to fixed fluxes diagnosed at the equilibrium does not change the equilibrium, used as an initial state. However, the same fixed-flux forcing applied to an ocean at rest (uniform temperature) produces perpetual oscillations in all the models except two (PGRW and PGS). In fact, a minimal temperature perturbation to the equilibrium state (0.1°C over 500 km $\times$ 500 km and 100 m deep) triggers oscillations under the same diagnosed fixed fluxes in all the models except PGRW and PGS. This clearly suggests that initial conditions are important and a subtle combination of parameters, initial state, and forcing gives rise to different model results in this study and the literature (Cai et al. 1995; GP96); however, most of the experiments in these previous studies were only initialized with the exact equilibrium state after the restoring experiments. The question whether the oscillation behavior depends on the initial state (same model, parameters, and forcing) is a fundamental issue: All the experiments that we carry

out confirm that, if the model does not remain in equilibrium upon switching to fixed flux boundary conditions (that is rather unlikely in the real ocean, considering the atmospheric synoptic activity or the radiative seasonal cycle), then the oscillations that become fully developed after a few hundred years have the same characteristics for the same parameters and forcing, whatever the initial temperature field was (like a mode of the mean circulation). The statistical characteristics of the oscillations that we discuss in the following are therefore robust, regardless of the initial state (see expts 82 vs 83 for instance).

The variability occurring in these models under constant surface heat fluxes (or under restoring boundary conditions with a long relaxation timescale as in section 6) is concentrated in the thermocline (upper 400 m), where temperature anomalies reach a few degrees. The pattern of variability is rather complex and varies widely depending on the forcing (section 5b): the largest variability usually remains concentrated in the north half, but in the northwest quarter with diagnostic fluxes. In the deeper layers, variability is greatly reduced and concentrated in convective regions along the polar boundary. The consequences of these temperature deviations on the model dynamics are always important in terms of meridional overturning (many Sverdrups) or poleward heat transport (0.05–0.2 petawatt). A typical evolution of the upper 250-m temperatures and velocities over a period is discussed in section 5d. The oscillation periods produced by the various models are in the interdecadal range (31 ± 15 yr).

3. Parameter sensitivity analysis

a. Methodology

We begin by comparing the variability found in models using either spherical or Cartesian coordinates. Since no major differences arise from the use of either coordinate system, we use Cartesian coordinates in all subsequent experiments in order to study the influence of β, the Coriolis parameter, the horizontal and vertical diffusion, the convective adjustment, the momentum dissipation, the horizontal and vertical discretization, the basin width, and the forcing amplitude. The forcing for all these experiments is the ''linear'' surface heat flux described in the last section. The numerous experiments are summarized in Table 1, and Table 2 provides various statistics for the mean circulation and its variability. The statistics are computed once the oscillatory state is regular—that is, when the diagnostic values averaged over an oscillation period remain constant (usually after 2000 yr). The temperature field is initialized at 4°C and the zero area average of the surface heat fluxes warrants that the mean basin temperature does not drift in time.

HC94 carried out a similar parameter sensitivity study for the haline circulation under the natural boundary condition for salt proposed by Huang (1993), which drives a very intense overturning cell sinking at low latitudes. Here, we extend this work for the thermally driven circulation, with fixed surface fluxes inducing a direct overturning cell of realistic amplitude. The comparison with their results is done whenever the same parameter is considered.

Different schemes for momentum dissipation and associated boundary conditions are used (HWC) to test the robustness of the conclusions we draw about the influence of processes and parameters. Since the characteristics of the oscillations are sensitive to the interaction of model parameterizations, resolution, parameters, and forcing, great care is exercised when different models produce different behaviors: only general conclusions are drawn. In most cases, the oscillatory behavior is robust in a large range of parameters and shows significant variations in terms of SST, velocities, or heat transport.

When the oscillations are not perfectly regular, the main period is estimated at the maximum of the power spectrum density through a Fourier transform of the mean surface temperature time series (an approximation symbol is then printed before the period value in Table 2). An oscillation index is defined on the temperature field, the only common ground between models with various dynamics, as the basin average of the standard deviation of temperature σ over one period if the oscillation is regular, otherwise over a long time compared to the estimated period:

$$\text{oscillation index} = \frac{1}{V}\iiint_V \sigma_{(x,y,z)}\, dV,$$

where

$$\sigma(x, y, z) = \sqrt{\frac{1}{\tau}\int_\tau (T(x, y, z, t) - \overline{T}(x, y, z))^2\, dt}$$

$$\overline{T}(x, y, z) = \frac{1}{\tau}\int_\tau T(x, y, z, t)\, dt.$$

In addition, traditional diagnostics (means and standard deviations) are given in Table 2: the total kinetic energy (KE), the maximum of the meridional overturning streamfunction (MO) and of the advective poleward heat transport (PHT), and the area-averaged surface and bottom temperature.

b. Spherical versus Cartesian coordinates

Spherical geometry is necessary for realistic modeling of the oceanic basin-scale thermohaline circulation. However, Cartesian coordinates are far more tractable and will be used for further parameter sensitivity analysis; we first justify the validity of Cartesian coordinates for studying these oscillations. We compare the mean thermohaline circulation and oscillatory behavior of a ''spherical'' ocean sector and a rectangular

Cartesian plane, both extending from 20° to 60°N with similar width at 40°N (expts 1 and 2). The forcing is the ''linear'' surface heat flux, zonally uniform and linearly varying with latitude, but whose area average is subtracted for the spherical coordinates experiment to ensure no drift of the mean basin temperature (the extrema become 40.4 and -49.6 instead of ± 45 W m^{-2}). In the Cartesian coordinates experiment (expt 2), the Coriolis parameter is set to $2\Omega \sin(\theta)$ such that the value of β is similar to the one in the spherical case for each latitude. All the models have been compared but only the results for PGL are given.

The convergence of meridians with latitude does not have dramatic consequences on the time-mean circulation, except a slight decrease in KE and PHT compared to the Cartesian experiments. Since the most energetic circulation (western boundary current and its extension as an eastward zonal jet in the polar region) takes place in the north half of the basin, where the spherical basin is the narrowest, the transports of mass and heat are lowered. There is no common modification in the oscillatory behavior among the various models: the periods change by a few years and the index by some 10^{-3} °C. The variability patterns (standard deviation of the upper 250-m temperature) are nearly identical (Figs. 1–2).

c. The influence of β

Winton (1996) showed that the β effect is not necessary for decadal variability to occur since an f plane reproduces the oscillatory behavior. This result is confirmed here (expts 3 and 5 to 9) and the influence of the Coriolis parameter is discussed in the next section. But first, we want to stress the relevance of the β-plane approximation for the analysis of the oscillations. Therefore we compare the last Cartesian experiment with β varying realistically (expt 2) to the control run (expt 0) on a Cartesian β plane centered at 40°N. There are very little differences between the mean states and variability patterns of these two configurations whatever the model used. However, setting β to zero has a significant influence on the variability and the mean state, by modifying the extreme values taken by the rotation rate and the horizontal divergence of geostrophic flows. The consequences are different between the various models: robust changes are a net increase in the mean meridional overturning and, consequently, in the mean bottom temperature (because of a reduced residence time at the surface). The change in the standard deviation patterns (Figs. 1 and 3) suggest that the β effect shifts the variability to the northern regions (where f is the strongest) and toward the western half (Rossby waves), whereas the stronger variability in the f-plane experiment is spread over all latitudes, with two extrema in the center of the northwest and southeast quarters of the basin. Nevertheless, in agreement with W96, we conclude that the β effect is not essential for the variability to occur or to set the decadal period.

d. Influence of the Coriolis parameter

The analysis of the variability in f-plane experiments is simpler because it removes the contribution of β to the vertical velocities, which are then determined through vertical integration of the divergence of the Reynolds stress (in the purely geostrophic model PGO, the vertical velocities thus cancel everywhere except along the boundaries). Then, it is straightforward to compare the influence of the geostrophic and ageostrophic velocities by varying the constant Coriolis parameter (expts 3 to 9). In all the models, the increase of the rotation rate reduces the part of the ageostrophic terms responsible for the nonzonal circulation: Consequently, KE, MO, and PHT decrease. Since the surface fluxes have more time to influence the surface temperature, colder waters arise in the northern regions, convect, and fill the bottom, whereas warmer surface temperatures (not mixed down by convection) raise the area average. In spite of a less energetic mean circulation, the oscillation amplitude and period increase with f. This suggests that the oscillations rely on the geostrophic balance rather than ageostrophic terms, in agreement with the conclusions regarding the damping influence of increasing the friction (section 3i).

The same conclusions apply when varying the mean Coriolis parameter on a β plane (expts 10 to 14). In addition, a nonrotating case is implemented, with both PGL (expt 4) and the MOM code: obviously not relevant to geophysical flows, these experiments show however that the resulting circulations, although highly energetic, do not sustain any oscillations—in fact, a steady state is achieved within a few years and evolves slightly on diffusive timescales afterward. In conclusion, the geostrophic balance is absolutely essential to the oscillatory behavior.

e. The damping effect of the horizontal diffusion

Horizontal tracer diffusion appears to be the most critical damping term for the variability. Whatever the model, forcing, and initial state, there is a critical value of K_H above which oscillations are damped out (varying between 800 and 2500 m^2 s^{-1} depending on the model used and the horizontal resolution). Estimations of horizontal (isopycnal) mixing from Lagrangian float trajectories and tracer budgets vary between 500 and 2500 m^2 s^{-1} depending on the region of the experiments (Freeland et al. 1975; Armi and Stommel 1983; Jenkins 1991; Ollitrault 1995), hence the ocean would be close to a marginally stable state regarding these oscillations. These values are also commonly used in coarse-resolution models, in which decadal oscillations do not always occur when constant flux forcing is applied. However, higher resolution (marginally eddy-resolving)

TABLE 1. Experiments summary. Geometry: (*f*) plane and (β) β plane, followed by centered latitude. Longitude extent: C = 5120 km, N = 2560 km, W = 10 240 km. Latitude extent: C = 20°–60°N, W = 20°–100°N, X = 20°S–100°N. Number of gridpoints: horizontally C = 32 × 28. Forcing: L zonally uniform fixed surface fluxes linearly varying with latitude (Cos for cosine profile) followed by extrema (W m^{-2}); R as restoring boundary conditions for surface temperature, followed by the extrema of equivalent atmospheric temperature (°C), whereas the restoring constant is given in the specifications; D for diagnosed fixed fluxes at the equilibrium of the associated restoring experiment. K_H, K_V: horizontal and vertical tracer diffusivities (e-4, e5 ≡ × 10^{-4}, × 10^{5}, respectively, for example). A_H: horizontal viscosity; the vertical viscosity A_V is zero except in the MOM runs when it is stated in the specifications.

All experiments are carried out with most of the models (MOM, PGL, PG0, PGR0, and PGRW) but only the results from the PGL experiments on a Cartesian β plane are presented, otherwise the name of the model used is stated in the specifications. PGL is a planetary geostrophic (PG hereafter) model with Laplacian viscosity and no-slip boundary conditions (Colin de Verdière 1986, 1988; Winton 1993), very similar to the GFDL Modular Ocean Model (Pacanowski 1995) for a midlatitude basin at coarse resolution; PGR is a PG model with linear Rayleigh friction and PG0 is a ''purely geostrophic'' model with implicit numerical boundary layers due to the imposed no-slip or free-slip boundary conditions (Zhang et al. 1992), as a limit of PGL or PGR when the friction coefficient tends to zero. PGRW and PGS allow tangential velocities along the lateral boundaries that are solved either through a vorticity equation (Winton 1993) or by relaxing the hydrostatic equation through a linear vertical friction (Salmon 1986, 1990), within the PG equations with linear Rayleigh friction.

Expt.	Geometry	Long ext.	Lat ext.	NX × NY	NZ	Forcing (W m^{-2})	K_H (m^2 s^{-1})	K_V (m^2 s^{-1})	A_H (m^2 s^{-1})	Specifications (model is PGL if not otherwise stated)
0	β40°N	C	C	C	15	L ± 45	700	le−4	1.5e5	Control run: PGL Cartesian coord. β plane
1	Spherical	40°	C	C	15	L 40/−50	700	le−4	1.5e5	PGL in spherical coordinates
2	Cartesian	C	C	C	15	L ± 45	700	le−4	1.5e5	PGL in Cartesian coordinates: $f = 2\Omega \sin(\theta)$
3	*f*40°N	C	C	C	15	L ± 45	700	le−4	1.5e5	PGL on *f* plane centered at 40°N
4	$f \equiv 0$	C	C	C	15	L ± 45	700	le−4	1.5e5	PGL with no rotation
5	*f*14°N	C	C	C	15	L ± 45	700	le−4	1.5e5	PGL on *f* plane centered at 14°N
6	*f*22°N	C	C	C	15	L ± 45	700	le−4	1.5e5	PGL on *f* plane centered at 22°N
7	*f*31°N	C	C	C	15	L ± 45	700	le−4	1.5e5	PGL on *f* plane centered at 31°N
8	*f*51°N	C	C	C	15	L ± 45	700	le−4	1.5e5	PGL on *f* plane centered at 51°N
9	*f*66°N	C	C	C	15	L ± 45	700	le−4	1.5e5	PGL on *f* plane centered at 66°N
10	β40° *f*26°N	C	C	C	15	L ± 45	700	le−4	1.5e5	β plane with β(40°N) but f(40°N) = 2Ω sin(26°)
11	β40° *f*32°N	C	C	C	15	L ± 45	700	le−4	1.5e5	β plane with β(40°N) but f(40°N) = 2Ω sin(32°)
12	β40° *f*57°N	C	C	C	15	L ± 45	700	le−4	1.5e5	β plane with β(40°N) but f(40°N) = 2Ω sin(57°)
13	β40° *f*74°N	C	C	C	15	L ± 45	700	le−4	1.5e5	β plane with β(40°N) but f(40°N) = 2Ω sin(74°)
14	β40° *f*90°N	C	C	C	15	L ± 45	700	le−4	1.5e5	β plane with β(40°N) but f(40°N) = 2Ω sin(90°)
15	β40°N	C	C	C	15	L ± 45	350	le−4	1.5e5	
16	β40°N	C	C	C	15	L ± 45	500	le−4	1.5e5	
17	β40°N	C	C	C	15	L ± 45	1000	le−4	1.5e5	
18	β40°N	C	C	C	15	L ± 45	1500	le−4	1.5e5	
19	β40°N	C	C	C	15	L ± 45	2000	le−4	1.5e5	
20	β40°N	C	C	C	15	L ± 45	2500	le−4	1.5e5	
21	β40°N	C	C	C	15	L ± 45	3000	le−4	1.5e5	
22	β40°N	C	C	C	15	L ± 45	0	le−4	1.5e5	Upstream horizontal advection scheme
23	β40°N	C	C	C	90	L ± 45	700	le−5	1.5e5	
24	β40°N	C	C	C	90	L ± 45	700	3e−5	1.5e5	
25	β40°N	C	C	C	15	L ± 45	700	3e−4	1.5e5	
26	β40°N	C	C	C	15	L ± 45	700	le−3	1.5e5	
27	β40°N	C	C	C	15	L ± 45	700	le−4	1.5e5	No convective adjustment
28	*f*40°N	C	C	C	15	L ± 45	700	le−4	1.5e5	No convective adjustment
29	β40°N	C	C	C	15	L ± 45	700	le−4	1.5e5	MOM: Laplacian + no-slip boundary cond.
30	β40°N	C	C	C	15	L ± 45	700	le−4	1.5e5	PGL: Laplacian + free-slip boundary cond.
31	β40°N	C	C	C	15	L ± 45	700	le−4	0.0	PGR0: linear friction + no-slip boundary cond.
32	β40°N	C	C	C	15	L ± 45	700	le−4	0.0	PGRslip: linear friction + free-slip boundary cond.
33	β40°N	C	C	C	15	L ± 45	700	le−4	0.0	PGRW: no-normal-flow boundary cond. (Winton 1993)
34	β40°N	C	C	C	90	L ± 45	700	le−4	0.0	PGS (Salmon 1986, 1990) $\epsilon_v = 0.03$
35	β40°N	C	C	C	90	L ± 45	700	le−4	0.0	PGS (Salmon 1986, 1990) $\epsilon_v = 0.3$
36	β40°N	C	C	C	15	L ± 45	700	le−4	0.0	PGslip: purely geostrophic + free-slip boundary cond.
37	β40°N	C	C	C	15	L ± 45	700	le−4	0.0	PG0: purely geostrophic + no-slip boundary cond.
38	β40°N	C	C	C	15	L ± 45	700	le−4	1.0e3	
39	β40°N	C	C	C	15	L ± 45	700	le−4	1.0e4	

TABLE 1. (*Continued*)

Expt	Geometry	Long ext.	Lat ext.	NX × NY	NZ	Forcing (W m^{-2})	K_H (m^2 s^{-1})	K_V (m^2 s^{-1})	A_H (m^2 s^{-1})	Specifications (model is PGL if not otherwise stated)
40	β40°N	C	C	C	15	L ± 45	700	le−4	5.0e4	
41	β40°N	C	C	C	15	L ± 45	700	le−4	1.0e5	
42	β40°N	C	C	C	15	L ± 45	700	le−4	5.0e5	
43	β40°N	C	C	C	15	L ± 45	700	le−4	1.0e6	
44	β40°N	C	C	C	15	L ± 45	700	le−4	1.5e5	MOM A_v = 1e−4 m^2 s^{-1}
45	β40°N	C	C	C	15	L ± 45	700	le−4	1.5e5	MOM A_v = 1e−3 m^2 s^{-1}
46	β40°N	C	C	C	15	L ± 45	700	le−4	1.5e5	MOM A_v = 1e−2 m^2 s^{-1}
47	β40°N	C	C	C	15	L ± 45	700	le−4	1.5e5	MOM A_v = 5e−2 m^2 s^{-1}
48	β40°N	C	C	C	15	L ± 45	700	le−4	1.5e5	MOM A_v = 7e−2 m^2 s^{-1}
49	β40°N	C	C	16 × 14	15	L ± 45	700	le−4	1.5e5	Low resolution
50	β40°N	C	C	24 × 21	15	L ± 45	700	le−4	1.5e5	Intermediate low resolution
51	β40°N	C	C	48 × 42	15	L ± 45	700	le−4	1.5e5	Intermediate high resolution
52	β40°N	C	C	64 × 56	15	L ± 45	700	le−4	1.5e5	High resolution
53	β40°N	C	C	C	90	L ± 45	700	le−4	1.5e5	dz = 50m × 90
54	β40°N	C	C	C	30	L ± 45	700	le−4	1.5e5	dz = 25 × 6,(50:25:250) × 2,275 × 6
55	β40°N	C	C	C	20	L ± 45	700	le−4	1.5e5	dz = 25 × 4, 50 × 4, 100:50:450, 500 × 4
56	β40°N	C	C	C	18	L ± 45	700	le−4	1.5e5	dz = 50 × 6, 100:50:450, 500 × 4
57	β40°N	C	C	C	15	L ± 45	700	le−4	1.5e5	dz = 100 × 4, 150:50:450, 500 × 4
58	β40°N	C	C	C	8	L ± 45	700	le−4	1.5e5	dz = 50, 100, 250, 450, 650, 850, 1100 × 2
59	β40°N	C	C	C	8	L ± 45	700	le−4	1.5e5	dz = 100 × 2, 200:200:1000, 1300
60	β40°N	C	C	C	8	L ± 45	700	le−4	1.5e5	dz = 100 × 2, 200:200:1000, 1300 upstream vert. adv.
61	β40°N	C	C	C	4	L ± 45	700	le−4	1.5e5	dz = 100, 300, 1000, 3100 upstream vert. adv.
62	β40°N	C	C	C	4	L ± 45	700	le−4	1.5e5	dz = 200, 400, 800, 3100 upstream vert. adv.
63	β40°N	C	C	C	2	L ± 45	700	le−4	1.5e5	dz = 250, 4250 upstream vert. adv.
64	β40°N	C	C	C	2	L ± 45	700	le−4	1.5e5	dz = 500, 4000 upstream vert. adv.
65	β40°N	C	C	C	15	L ± 5	700	le−4	1.5e5	
66	β40°N	C	C	C	15	L ± 15	700	le−4	1.5e5	
67	β40°N	C	C	C	15	L ± 30	700	le−4	1.5e5	
68	β40°N	C	C	C	15	L ± 60	700	le−4	1.5e5	
69	β40°N	C	C	C	15	L ± 90	700	le−4	1.5e5	
70	β40°N	C	C	C	15	L ± 135	700	le−4	1.5e5	
71	β40°N	N	C	16 × 28	15	L ± 45	700	le−4	1.5e5	Basin 50% narrower
72	β40°N	W	C	48 × 28	15	L ± 45	700	le−4	1.5e5	Basin 50% wider
73	β40°N	W	C	64 × 28	15	L ± 45	700	le−4	1.5e5	Basin twice wider (Pacific)
74	β40°N	W	C	64 × 28	15	L ± 45	700	le−4	1.5e5	Zero heat flux on eastern half
75	β40°N	C	W	32 × 56	15	L ± 45	700	le−4	1.5e5	Zero heat flux on northern half
76	*f*40°N	C	W	32 × 56	15	Cos ± 45	700	le−4	1.5e5	Forcing = cosine symmetric/40°N
77	*f*40°N	C	C	C	15	Cos ± 45	700	le−4	1.5e5	Forcing = cosine (half wave)
78	β40°N	C	W	32 × 56	15	L ± 45	700	le−4	1.5e5	Zero heat flux on southern half
79	β40°N	W	C	64 × 28	15	L ± 45	700	le−4	1.5e5	Zero heat flux on western half
80	β40°N	C	C	C	15	L ± 45	500	le−4	1.5e5	Periodic channel in the east–west direction
81	β40°N	C	C	C	15	R 25:2°C	700	le−4	1.5e5	$Q_H = (T^* - T) \times 35$ W m^{-2} K^{-1} (Haney 1971)
82	β40°N	C	C	C	15	D exp.81	700	le−4	1.5e5	Init.: T@equilibrium from experiment 81
83	β40°N	C	C	C	15	D exp.81	700	le−4	1.5e5	Init.: $T \equiv 4$°C
84	*f*40°N	C	C	C	15	R 25:2°C	700	le−4	1.5e5	$Q_H = (T^* - T) \times 35$ W m^{-2} K^{-1} (Haney 1971)
85	*f*40°N	C	C	C	15	D exp.84	700	le−4	1.5e5	Init.: T@equilibrium from experiment 84
86	β40°N	C	C	C	15	R 29:−2°C	700	le−4	1.5e5	$Q_H = (T^* - T) \times 10$ W m^{-2} K^{-1} (Seager et al. 1995)
87	β40°N	C	C	C	15	L ± 45	100	le−4	1.5e5	MOM isopycnal mixing 700 m^2 s^{-1}
88	β40°N	C	C	C	15	L ± 45	0	le−4	1.5e5	MOM isopycnal mixing 700 m^2 s^{-1} + GM1000 m^2 s^{-1}
89	β40°N	C	C	C	15	L ± 45	700	le−4	1.5e5	MOM GM90 1000 m^2 s^{-1}
90	β40°N	C	C	C	15	L ± 45	700	le−4	1.5e5	Wind forcing
91	β40°N	C	C	C	15	L ± 45	700	le−4	1.5e5	Seasonal cycle in surface heat flux

TABLE 2. Variability diagnostics for the experiments detailed in Table 1. Oscillation period (yr) (a ~ prefix means irregular oscillation), oscillation index (10^{-3} °C) as defined in section 3, time average and standard deviation of kinetic energy density (0.1 J m^{-3}), meridional overturning (Sv $\equiv 10^6$ m^3 s^{-1}), maximum advective poleward heat transport (PW = 10^{15} W), area-averaged surface (0–50 m) and bottom (3950–4500 m) temperatures (°C). Note that in the fixed flux experiments only, the mean basin temperature is set to 4°C by initial conditions.

Expt	Specific. (short) (m^2 s^{-1})	Oscil. period (yr)	Oscil. index (10^{-3} K)	KE mean (0.1 J m^{-3})	KE st.dev (0.1 J m^{-3})	MO mean (Sv)	MO st.dev (Sv)	PHT mean (PW)	PHT st.dev (PW)	Tsurface mean (°C)	Tsurf st.dev (°C)	Tbott. mean (°C)	Tbott. st.dev (°C)
0	β40°N	25.4	41.8	0.286	0.046	8.08	0.90	0.254	0.025	13.776	0.091	3.183	0.0012
1	Spherical	23.3	36.8	0.254	0.038	8.44	0.96	0.239	0.022	13.443	0.084	3.227	0.0009
2	Cartesian	25.1	34.4	0.286	0.045	8.16	0.90	0.253	0.023	13.740	0.087	3.201	0.0012
3	*f*40°N	~24.9	96.3	0.289	0.083	7.99	1.85	0.259	0.051	12.034	0.182	3.352	0.0049
4	$f \equiv 0$	0.0	0.0	1.299	0.000	44.92	0.00	0.267	0.000	5.811	0.000	3.944	0.0000
5	*f*14°N	12.1	70.1	0.473	0.148	15.64	6.94	0.278	0.111	10.340	0.203	3.515	0.0003
6	*f*22°N	~17.4	94.7	0.401	0.127	12.21	5.02	0.266	0.065	11.047	0.231	3.516	0.0063
7	*f*31°N	~20.2	98.5	0.345	0.111	9.13	2.78	0.264	0.059	11.592	0.209	3.424	0.0079
8	*f*51°N	~25.9	89.3	0.260	0.064	7.42	1.43	0.257	0.037	12.433	0.146	3.277	0.0086
9	*f*66°N	73.0	121.0	0.225	0.048	7.49	1.40	0.257	0.026	12.556	0.158	3.274	0.0037
10	β40° *f*26°N	17.1	47.5	0.331	0.059	10.29	2.15	0.258	0.033	13.499	0.092	3.295	0.0025
11	β40° *f*32°N	22.3	31.4	0.305	0.043	8.81	1.02	0.254	0.024	13.670	0.080	3.236	0.0008
12	β40° *f*57°N	32.0	49.4	0.252	0.046	8.00	0.95	0.254	0.027	13.792	0.100	3.104	0.0012
13	β40° *f*74°N	38.5	59.2	0.214	0.036	7.32	0.60	0.252	0.027	14.110	0.124	3.040	0.0026
14	β40° *f*90°N	45.7	64.0	0.187	0.029	7.21	0.48	0.251	0.026	14.310	0.131	2.987	0.0031
15	$K_H = 350$	~25.0	118.4	0.337	0.079	9.65	2.47	0.270	0.053	13.833	0.211	3.193	0.014
16	$K_H = 500$	~21.2	131.5	0.312	0.101	8.85	3.00	0.271	0.064	13.873	0.260	3.139	0.0093
17	$K_H = 1000$	28.8	32.7	0.239	0.028	9.69	0.67	0.250	0.022	13.644	0.085	3.238	0.0015
18	$K_H = 1500$	31.1	50.6	0.191	0.021	11.90	0.78	0.243	0.021	13.361	0.096	3.315	0.0023
19	$K_H = 2000$	30.7	38.4	0.161	0.009	12.39	0.58	0.234	0.011	13.015	0.052	3.365	0.0016
20	$K_H = 2500$	0.0	0.0	0.137	0.000	12.69	0.02	0.223	0.000	12.709	0.001	3.403	0.0000
21	$K_H = 3000$	0.0	0.0	0.117	0.000	12.95	0.00	0.213	0.000	12.468	0.000	3.427	0.0000
22	Upstream hor adv	~32.5	62.9	0.434	0.035	8.90	0.50	0.255	0.016	13.901	0.101	3.194	0.0025
23	K_v = le−5	0.0	0.0	0.079	0.000	4.00	0.00	0.253	0.000	30.959	0.000	3.270	0.0007
24	K_v = 3e−5	20.7	17.7	0.142	0.011	5.70	0.25	0.253	0.015	21.125	0.088	3.213	0.0006
25	K_v = 3e−4	35.1	84.4	0.539	0.132	12.96	2.43	0.254	0.039	9.538	0.091	3.171	0.0022
26	K_v = le−3	42.7	200.0	1.072	0.388	22.07	8.54	0.258	0.092	6.782	0.126	3.264	0.0154
27	No conv	~33.0	107.0	0.346	0.104	9.50	3.03	0.262	0.051	12.670	0.292	3.225	0.0130
28	*f*40NoConv	~65.0	125.4	0.316	0.111	8.48	3.30	0.263	0.042	10.864	0.367	3.342	0.0156
29	MOM	26.1		0.263	0.046	9.26		0.282		13.632		3.188	
30	PGLslip	37.4	105.0	0.294	0.062	8.33	1.83	0.260	0.040	13.213	0.211	3.243	0.0015
31	PGR0	24.6	29.3	0.215	0.027	8.55	0.52	0.254	0.015	14.646	0.064	3.167	0.0011
32	PGRslip	44.3	85.2	0.180	0.029	8.65	1.61	0.254	0.026	14.097	0.157	3.264	0.0020
33	PGRW	34.0	30.1	0.302	0.025	7.14	0.65	0.255	0.015	13.405	0.101	3.348	0.0003
34	PGS 0.03	35.0	31.3	0.293	0.025	7.05	0.66	0.254	0.016	13.332	0.106	3.331	0.0002
35	PGS 0.3	0.0	0.0	0.276	0.000	6.78	0.00	0.254	0.000	13.462	0.000	3.356	0.0000
36	PGslip	~45.7	29.6	0.587	0.047	10.86	1.20	0.291	0.062	13.167	0.074	3.321	0.0038
37	PG0	32.3	56.0	1.033	0.152	8.70	1.04	0.248	0.020	13.318	0.078	3.094	0.0011
38	A_H = le3	31.6	48.8	0.914	0.135	8.43	0.97	0.248	0.020	13.359	0.078	3.100	0.0011
39	A_H = le4	29.7	43.6	0.594	0.095	7.85	0.74	0.249	0.021	13.450	0.084	3.128	0.0011
40	A_H = 5e4	28.6	40.4	0.393	0.071	7.66	0.79	0.251	0.024	13.652	0.094	3.148	0.0010
41	A_H = le5	26.9	37.8	0.325	0.056	7.81	0.84	0.252	0.025	13.749	0.094	3.165	0.0011
42	A_H = 5e5	22.7	35.0	0.194	0.018	12.61	1.36	0.257	0.022	13.744	0.089	3.277	0.0012
43	A_H = le6	20.4	36.1	0.150	0.015	15.05	2.39	0.258	0.028	13.943	0.121	3.285	0.0005
44	A_v = le−4	26.1		0.263	0.046	9.26		0.282		13.632		3.188	
45	A_v = le−3	26.0		0.263	0.045	7.05		0.239		13.570		3.188	

TABLE 2. (*Continued*)

Expt	Specific. (short) (m^2 s^{-1})	Oscil. period (yr)	Oscil. index (10^{-3} K)	KE mean (0.1 J m^{-3})	KE st.dev (0.1 J m^{-3})	MO mean (Sv)	MO st.dev (Sv)	PHT mean (PW)	PHT st.dev (PW)	Tsurface mean (°C)	Tsurf st.dev (°C)	Tbott. mean (°C)	Tbott. st.dev (°C)
46	A_v = 1e−2	26.0		0.261	0.045	8.33		0.260		13.726		3.187	
47	A_v = 5e−2	25.7		0.249	0.039	7.96		0.246		13.904		3.192	
48	A_v = 7e−2	25.8		0.245	0.038	6.78		0.224		13.823		3.195	
49	16 × 14	28.3	25.3	0.336	0.032	9.94	0.93	0.266	0.018	13.721	0.074	3.267	0.0014
50	24 × 21	26.4	44.1	0.311	0.058	7.99	1.22	0.258	0.032	13.857	0.112	3.169	0.0010
51	48 × 42	25.4	37.9	0.262	0.028	8.89	1.16	0.250	0.019	13.594	0.068	3.219	0.0016
52	64 × 56	26.2	39.7	0.266	0.036	9.26	0.96	0.250	0.020	13.418	0.083	3.215	0.0015
53	nz = 90(50)	26.3	40.8	0.281	0.048	8.16	0.97	0.253	0.026	13.705	0.095	3.165	0.0009
54	nz = 30	26.1	39.7	0.282	0.047	8.28	0.96	0.252	0.025	14.073	0.093	3.171	0.0008
55	nz = 20(25)	26.0	38.0	0.284	0.048	8.04	1.02	0.253	0.026	14.085	0.095	3.179	0.0011
56	nz = 18	25.9	38.2	0.283	0.048	8.02	0.99	0.253	0.026	13.712	0.095	3.179	0.0011
57	nz = 15′	26.1	38.3	0.281	0.048	8.02	1.01	0.254	0.026	13.025	0.093	3.179	0.0010
58	nz = 8	11.0	21.8	0.315	0.004	10.36	0.77	0.254	0.017	13.894	0.014	3.228	0.0007
59	nz = 8′	14.3	34.8	0.294	0.012	9.58	0.52	0.255	0.010	13.007	0.013	3.228	0.0007
60	nz = 8′Upz	33.0	87.0	0.436	0.117	16.56	4.30	0.258	0.045	11.399	0.153	3.243	0.0022
61	nz = 4:Upz	43.8	143.0	0.745	0.174	32.21	6.01	0.259	0.039	10.324	0.156	3.530	0.0070
62	nz = 4′Upz	40.2	124.0	0.654	0.162	27.78	5.89	0.256	0.040	9.494	0.111	3.442	0.0066
63	nz = 2:Upz	83.3	191.0	2.128	0.277	25.14	3.12	0.270	0.034	6.485	0.070	3.854	0.0041
64	nz = 2′Upz	63.7	211.0	2.228	0.520	35.89	6.09	0.270	0.048	5.720	0.095	3.785	0.0120
65	Q_H = 5	100.5	7.2	0.030	0.002	5.90	0.44	0.026	0.001	5.695	0.013	3.792	0.0006
66	Q_H = 15	57.6	32.7	0.098	0.017	7.42	0.96	0.083	0.011	8.184	0.066	3.572	0.0013
67	Q_H = 30	35.4	33.9	0.193	0.031	7.75	0.82	0.168	0.018	11.173	0.076	3.348	0.0013
68	Q_H = 60	~18.6	93.0	0.363	0.082	9.23	2.15	0.346	0.058	16.122	0.194	3.046	0.0032
69	Q_H = 90	~17.8	182.0	0.520	0.147	10.88	3.41	0.536	0.108	20.572	0.381	2.782	0.0163
70	Q_H = 135	~16.5	212.0	0.747	0.183	12.77	3.54	0.810	0.150	26.386	0.470	2.532	0.0280
71	L_x50%	19.3	33.8	0.193	0.041	5.62	1.21	0.129	0.017	12.736	0.120	3.392	0.0008
72	L_x150%	29.0	51.7	0.370	0.038	11.90	1.39	0.380	0.033	14.589	0.065	3.026	0.0015
73	L_x200%	38.1	85.0	0.456	0.077	14.41	2.01	0.501	0.065	15.307	0.097	2.844	0.0030
74	be0.hf	37.5	56.5	0.195	0.043	11.57	2.99	0.251	0.050	9.811	0.107	3.273	0.0013
75	bn0.hf	37.0	87.4	0.159	0.048	8.52	2.78	0.262	0.069	9.267	0.135	3.484	0.0034
76	*f*40cosym	~40.0	292.2	0.410	0.129	7.04	3.39	0.324	0.064	13.441	0.419	3.070	0.0240
77	*f*40.coshf	~28.0	136.0	0.331	0.117	8.21	2.51	0.326	0.067	13.096	0.257	3.320	0.0142
78	bs0.hf	29.0	56.0	0.300	0.048	21.03	5.32	0.253	0.055	11.184	0.096	2.885	0.0050
79	bw0.hf	28.4	27.5	0.167	0.005	17.56	1.38	0.242	0.008	11.940	0.005	3.175	0.0007
80	X-periodic	16.1	85.5	36.477	0.555	2.33	0.14	0.096	0.006	31.275	0.292	−3.042	0.1605
81	35R25:2°	0.0	0.0	0.275	0.000	15.45	0.00	0.222	0.000	13.499	0.000	3.539	0.0000
82	Diag. flux	23.0	56.5	0.290	0.065	12.68	4.40	0.224	0.042	13.889	0.107	3.423	0.0014
83	df.init4°C	23.0	56.6	0.289	0.064	12.67	4.41	0.224	0.041	13.890	0.107	3.424	0.0012
84	*f*40R25:2°	0.0	0.0	0.384	0.000	21.73	0.00	0.290	0.000	13.500	0.000	3.688	0.0000
85	*f*40.df	~19.3	80.5	0.363	0.055	16.93	5.09	0.288	0.035	13.725	0.129	3.584	0.0081
86	10R29:−2°	28.7	33.0	0.238	0.026	9.52	1.32	0.203	0.022	13.515	0.038	4.671	0.0144
87	ISOPYC.	~20.1		0.354	0.077	12.25		0.327		14.293		3.112	
88	GM90	15.6		0.165	0.010	8.26		0.242		13.859		3.312	
89	GMHOR.	20.8		0.136	0.020	7.81		0.208		13.633		3.212	
90	PGL wind	25.1	50.0	0.668	0.097	7.55	1.74	0.253	0.040	12.744	0.077	3.085	.0011
91	Seas. cyc.	25.0	49.0	0.306	0.114	10.52	3.12	0.258	0.035	12.918	0.207	2.879	.0054

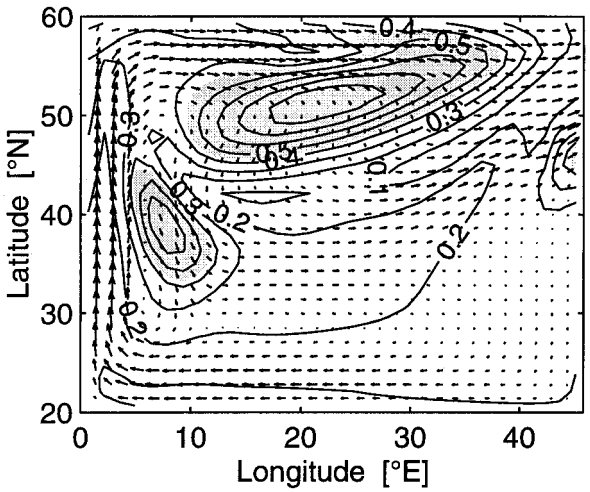

FIG. 1. Standard deviation of the upper 250-m temperature (°C) for the control run (expt 0): PGL under the ''linear'' surface heat flux (zonally uniform and linearly varying with latitude from 45 W m^{-2} at 20°N to -45 W m^{-2} at 60°N) on a Cartesian coordinates β plane centered at 40°N. Regions of variability greater than the area mean plus the standard deviation are shaded. The time-averaged velocity field is superimposed [the scale is 3 cm s^{-1} $(deg)^{-1}$].

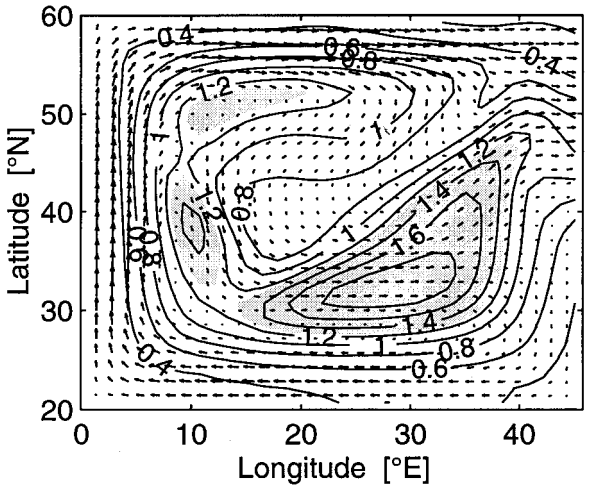

FIG. 3. Standard deviation of the upper 250-m temperature (°C) for PGL under the ''linear'' surface heat flux on a Cartesian coordinate f plane centered at 40°N (expt 3).

models, where horizontal mixing is actually carried out by eddies generated by baroclinic instabilities, seems to reproduce the decadal variability as well (Fanning and Weaver 1998). Horizontal diffusion also controls the regularity of the oscillation, its amplitude, and period (Fig. 4). In all the models, increasing the horizontal diffusion smooths the horizontal gradients of temperature and reduces the horizontal velocities, hence the mean KE (Bryan 1987). As the diffusivity increases, the diffusive part of the PHT increases, the deep waters warm while the surface waters cool. This follows since diffusion at high latitudes (where gradients are strong) artificially transports warm waters poleward into the convection regions, thus forming relatively warm bottom water. Reduced surface temperatures then allow conservation of the fixed basin heat content. Regarding the variability, increasing K_H lengthens the oscillation period and reduces its amplitude. These results are consistent with the conclusions of HC94.

As an alternative to the centered difference advection scheme and explicit horizontal diffusion, we implement an upstream advection scheme in the horizontal, with no explicit diffusion (expt 22): the implicit diffusion of such a scheme is $U\Delta x/2$, reaching 10^3 m^2 s^{-1} for $U =$ 1 cm s^{-1} and $\Delta x = 160$ km. This approach of reducing the explicit uniform diffusion boosts the variability in all the models, in agreement with an average numerical

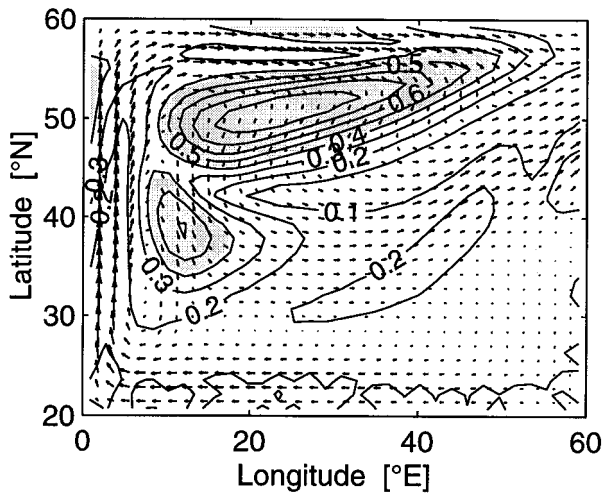

FIG. 2. Standard deviation of the upper 250-m temperature (°C) for PGL under the ''linear'' surface heat flux in spherical coordinates (expt 1).

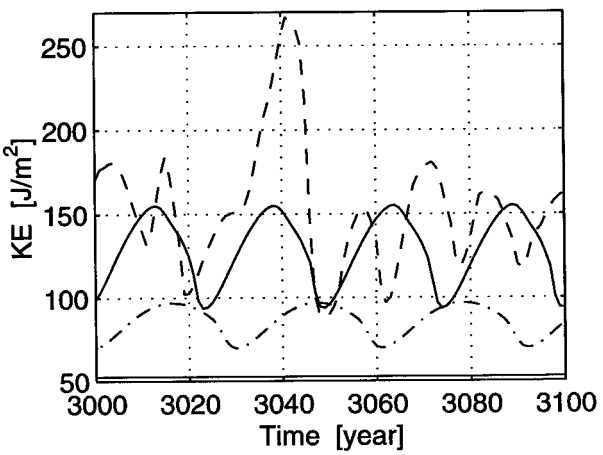

FIG. 4. The influence of horizontal diffusivity on the oscillatory behavior in the standard PGL experiment: Kinetic energy density as a function of time for $K_H = 350$ (expt 15, dashed), 700 (control run, solid), 1500 (expt 18, dash–dotted), and 3000 (expt 21, solid and constant) m^2 s^{-1}.

diffusion lower than the previous explicit value. The oscillation is thus robust to such a simple numerically derived velocity-dependent parameterization of horizontal mixing, where the horizontal eddy diffusivity is increased in regions of strong currents (where more eddies are likely to be generated by baroclinic or inertial instability).

The strong influence of horizontal diffusion is in agreement with the advective processes (e.g., Weaver and Sarachik 1991) where density anomalies travel in the polar regions and modify convection, hence the strength of the thermohaline circulation. When diffusion is too strong, these anomalies are diffused before reaching the convection regions, analogous to when too fast a relaxation is applied to the surface temperature and thereby damps out any SST deviations. Similarly, Chen and Ghil (1996) show that in an ocean model coupled to an atmospheric energy-balanced model, the oscillation amplitude is strongly dependent on the horizontal diffusion coefficient for the atmospheric temperature (playing a role similar to horizontal eddy diffusivity in the ocean for the damping of SST anomalies).

f. The driving effect of the vertical diffusion

Vertical diffusion plays a crucial role in driving the overturning thermohaline cell within differential surface heating. While potential energy is removed by convection and frictional dissipation, the explicit vertical mixing of buoyancy raises the center of gravity of a stably stratified density distribution yielding an increase of PE: this is actually the main source of PE when no wind-induced mixing is considered (see HWC). Within the internal thermocline traditional balance (Munk 1966), the vertical diffusion of heat equals the upward transport of cold water across the thermocline: Therefore, a tight dependency of the strength of the overturning circulation is expected. The scaling of the thermocline equations (detailed in the appendix) shows indeed a dependency of the meridional overturning in $K_v^{1/2}$ under fixed-flux boundary conditions. In fact, we find fit ranging from $K_v^{0.37}$ to $K_v^{0.46}$ depending on the model. A spatially uniform vertical mixing allows only a narrow range of diffusivity coefficients to obtain a realistic overturning: Since the area of our upwelling region is far smaller than the real ocean regions where North Atlantic Deep Water upwells, we need to use a vertical diffusivity larger than the values estimated from tracer release experiments in the thermocline (Ledwell et al. 1993). The sensitivity analysis of the oscillatory behavior with respect to K_v is therefore strongly linked to the sensitivity of the variability to the strength of the thermohaline circulation since a more energetic circulation is more likely to develop instabilities. Only the comparison with the role of the surface heat flux amplitude (section 3l) allows one to separate the influence of K_v from the effect of the stronger circulation.

We run all the models for K_v varying from 10^{-5} to 10^{-3} m^2 s^{-1}. The mean circulation evolves as expected: with increasing K_v, KE and meridional overturning increase strongly. More vertical mixing of the warm subtropical thermocline induces a cooling of the surface temperature in this area, whereas the subpolar temperatures mixed vertically by convection do not change much: thus, the mean surface temperature decreases strongly. The mean bottom temperature, depending principally on the surface water properties in the convection regions, increases slightly. Irregular changes in the variability at lower K_v made us rerun the simulations with increased vertical resolution (90 levels 50 m deep for expts 23 and 24) and the results changed significantly (Yin and Fung 1991). Only the lowest diffusion does not sustain the variability and reach a steady state after 1500 years. With stronger vertical mixing, the variability of the temperature field and of all the diagnostics increases regularly, and faster than linearly, whereas the oscillation period lengthens (from 21 to 43 yr for PGL). These conclusions are in agreement with HC94, although the meridional cell is always much stronger in their study: of the order of 100 Sv (Sv $\equiv 10^6$ m^3 s^{-1}).

g. The damping influence of the convective adjustment

Coarse-resolution ocean models cannot resolve the very short time and spatial scales of open-ocean convection. Therefore, it is parameterized independently of the advection–diffusion scheme by instantaneous vertical mixing of unstably stratified grid boxes at each time step. HWC showed that this process accounts for 30%–60% of the potential energy depletion (this is incidentally the computational cost of this routine as well). Marotzke (1991) noted that the numerical method used for this adjustment influences the stability of the thermohaline circulation under mixed boundary conditions. Cessi (1996) pointed out a grid-scale instability induced by such instantaneous convective adjustment. To assess the robustness of the oscillations to the convection scheme, we ran each model with convective adjustment removed. This is not physically appropriate since static instabilities now remain in the density fields, but it proves that the variability is not sustained by the convective adjustment algorithm.

Without convection, the mean circulation is much more energetic since horizontal density gradients, no longer mixed down, are enhanced (expts 27 vs 0, 28 vs 3 for PGL on β and f plane): the mean KE, MO, and PHT are increased. However, less cooling reaches the bottom waters, which subsequently warm. The upper layers cannot export their colder waters to depth as efficiently and cools. PGRW is the only model whose behavior does not change dramatically with or without convection. This is probably related to the high contribution of the KE dissipation in the potential energy depletion (in HWC, the role of convection in this model was half smaller than in the others: downward vertical

velocities efficiently drove the coldest water to depth). More relevant to our variability study, the regular oscillations observed in most of the models with convection now become chaotic, although the most energetic timescales inferred by Fourier analysis remain in the decadal range, usually longer than the period with convection. The amplitude of the oscillations increases strongly, as well as the standard deviations of all the diagnostics. These results suggest that the convection algorithm does not have a driving role in the variability, but rather acts as a damping term by mixing negative temperature anomalies downward. This is also done by vertical velocities, especially along the boundaries: without convection, these velocities are even more intense and contribute more efficiently to the vertical transport of heat and mass, but not enough to balance for the missing convection.

h. *Influence of the momentum dissipation parameterization and associated boundary conditions*

The momentum dissipation and associated boundary conditions significantly influence the mean circulation and deep-water characteristics of a thermohaline circulation model forced by restoring boundary conditions (HWC). This influence is verified here under fixed-flux boundary conditions (expts 29–37): The oscillation period and index vary widely depending on the choice of the viscosity scheme and the closure for tangential velocities along the boundaries. However, the differences among the time-averaged circulations are not as pronounced under this zonally uniform forcing as under restoring boundary conditions where the zonally and meridionally averaged circulations, as well as deep water properties, were principally related to the upwelling along the western boundary (HWC). There, the most intense surface fluxes occurred and had to be compensated, by upwelling of cold deep water when the dynamics makes it possible. Thus, for poleward heat transport comparable to the restoring runs, the time-averaged meridional overturning varies between 6.8 and 10.9 Sv instead of 7.6 and 15.6 Sv, but the ordering of the models remains almost the same. The range of variation of the mean bottom temperature is also reduced, but there is no significant correlation with the meridional overturning ($r = -0.3$). The influence of each momentum dissipation scheme or boundary condition on the oscillation features is difficult to rationalize: Free-slip boundary conditions significantly increase the oscillation amplitude and period with Rayleigh or Laplacian viscosity, but increase as well the nonlinearity of the oscillation (as shown by less sinusoidal time evolution).

i. *The damping influence of friction*

The influence of the friction coefficient is similar, whether the dissipation operator is linear on the horizontal (ε_H in PGRO) or the vertical (ε_V in PGS) or harmonic (horizontal A_H in PGL, vertical A_V in MOM). Increasing the viscosity coefficient always reduces the mean KE. Increasing horizontal viscosity (expts 37 to 43) usually increases the meridional overturning and slightly the advective poleward heat transport, whereas increasing the vertical friction (expt 34 vs 35, and 44–48) reduces the meridional cell intensity and very weakly the PHT. Both bottom and surface waters slightly warm: this paradox implies a less stratified thermocline resulting from more vertical mixing induced by enhanced ageostrophic circulation. Increasing the friction coefficient has the opposite effect on the oscillation from increasing the Coriolis parameter (section 3d): the period shortens and the amplitude decreases (oscillation index and all diagnostics standard deviations except the meridional overturning). We observe here more sensitivity to the mixing of momentum than suggested by HC94 (only the decrease of the mean KE with increased viscosity agrees with their study). The sensitivity of the variability to the vertical mixing of momentum is weak, in spite of the large range of viscosity coefficients tested ($A_V = 0$–0.07 m^2 s^{-1} in the MOM), as expected from the large predominance of horizontal viscosity (for numerical reasons): the amplitude of KE variations changes by less than 20% whereas the period changes by less than a year.

j. *Influence of the horizontal resolution*

The various models do not respond the same way when horizontal resolution is changed (expts 49 to 52 for PGL). Since some of them (PG0, PGR0, and PGRW) implement ''numerical'' boundary layers that do not allow a convergence of the circulation when resolution is increased, the mean circulation varies accordingly. The mean KE, MO, and advective PHT usually decrease slightly, as well as the mean bottom water temperature, with increasing resolution. However, the oscillation behavior is quite robust: the period and the oscillation index vary slightly with finer resolution. The other diagnostics vary irregularly and unpredictably. In addition to the modifications to the mean circulation depending on the resolution, one must consider the variation of the grid Peclet number ($U\Delta x/K_H$) when resolution, but not the model parameters, is changed: diffusion seems promoted relative to advection when the grid spacing is reduced. Curiously, HC94 found the oscillations very sensitive to the horizontal resolution in their model: this may be a consequence of the strong amplitude and variability of the meridional overturning driven by their natural salt boundary condition.

Below 100-km grid spacing, the planetary geostrophic approximation is no longer justified and we observe discrepancies with the primitive equations (PE) dynamics. With higher resolution, PE models induce variability more easily and with larger amplitude, suggesting that the nonlinear terms or time derivatives in the momentum

equations provide more inertia to the anomalies. This important issue is being investigated and will be reported in the near future.

k. The sensitivity to the vertical discretization

The influence of the vertical discretization is weak when we increase the resolution and the number of levels from the control 15-level run (expts 53 to 57) but quite important if we try to reduce it (expts 58 to 64). First, this confirms that the choice of vertical discretization used throughout this study is satisfying in terms of the oscillation characteristics presented in Table 2. However, reducing the number of levels and increasing the upper-level thicknesses leads to strong distortions in the variability and the mean state of the thermohaline circulation. In PGL, the use of 8 levels instead of 15 in the ''linear'' flux case halves the period and the oscillation index, whereas in PGR0, it suppresses the variability. When fewer levels are used, the variation of the level thickness with depth is too important, and numerical problems arise when centered differencing is used for the vertical advection: sources of cold water appear at middepth along the boundaries where vertical velocities are maximum (Bryan et al. 1975; Weaver and Sarachik 1990; Yin and Fung 1991). In such cases, an upstream scheme is used for the vertical advection, but the associated implicit vertical diffusion strongly increases the energy of the thermohaline circulation and the overturning rate, as well as the amplitude and period of the oscillations. Even a two-level discretization reproduces the oscillatory behavior and the variability pattern: such a simple configuration proved very useful in the study for the underlying oscillation mechanism.

l. Influence of the forcing amplitude

Scaling arguments (detailed in the appendix) show a dependency of the meridional overturning with the amplitude of the surface heat flux to the power ¼, which agrees fairly well with the numerical experiments (65 to 70) where the linear forcing varies from ± 5 to ± 135 W m^{-2}: The best fit for the overturning as a function of the forcing amplitude are obtained for regression coefficients varying from 0.17 to 0.32 (depending on the models: 0.22 for PGL and on average) in log–log plot. The mean circulation is increasingly energetic when the heat flux extrema are increased (KE, MO, and PHT). The mean surface temperature increases with the stronger warming of the thermocline, whereas the mean bottom temperature decreases with the more intense cooling at high latitudes. The oscillation amplitude increases regularly with the stronger thermohaline circulation (standard deviations of temperature, KE, and overturning), similarly to the effect of increasing the vertical mixing. However, the period of the oscillation evolves oppositely since it becomes shorter with increased forcing amplitude. This is reminiscent of the dependence of planetary wave speeds upon stratification: weaker stratification, associated with higher vertical mixing or lower vertical density gradient (lower forcing amplitude), induces slower waves that imply longer adjustment and oscillation periods.

m. Influence of the basin width

The sensitivity of the oscillation to the zonal extent of the basin is important to provide hints in the mechanism setting the period for the variability. The analysis of the response of a stratified but resting ocean to large-scale or stochastic wind forcing shows that the time required for the adjustment by Rossby waves depends linearly on the basin width (Anderson and Gill 1975; Frankignoul et al. 1997). However, varying the zonal extent of our model basin from 2560 km to 10 240 km (along with the number of grid points to keep the resolution constant) shows a dependency of the period with the width in a 0.46 power law (expts 71–73 for PGL). As the basin is extended zonally, the time-mean meridional overturning increases (in good agreement with the scaling given in the appendix) as well as KE and PHT, whereas the mean surface temperature increases to balance the colder deep waters formed farther east along the northern boundary. Meanwhile, the oscillations amplitude and period increase as well as the standard deviation of KE and PHT (it is not systematic for MO). Thus, wider basins produce stronger oscillations with longer periods, increasing roughly as the square root of the width (instead of proportionally, as would be the case for a mode of the basin width, given fixed stratification and zonal circulation).

4. The role of the boundaries

a. Motivation

Winton (1996) and GP96 proposed a boundary wave (viscous analog of Kelvin waves) mechanism that would achieve the appropriate timescale when propagating along the weakly stratified boundaries. However, these two studies did not agree on which boundaries are necessary. Although both suggested that the wave does not need to propagate around the whole basin to sustain the oscillations, W96 saw the source of the variability in the northeast corner of the basin, where the eastward zonal jet extending the western boundary current sinks along the eastern boundary. He presented a convincing description of a perturbation propagating eastward along the northern boundary with the right timescale. GP96, in a systematic analysis of the role of each boundary, concluded that the western boundary is the only important one for perpetuating the oscillations. In order to shed light on this issue, we analyze the influence of each boundary successively and show that none of these is fundamental to the oscillatory behavior. To eliminate the western boundary current, we finally perform an

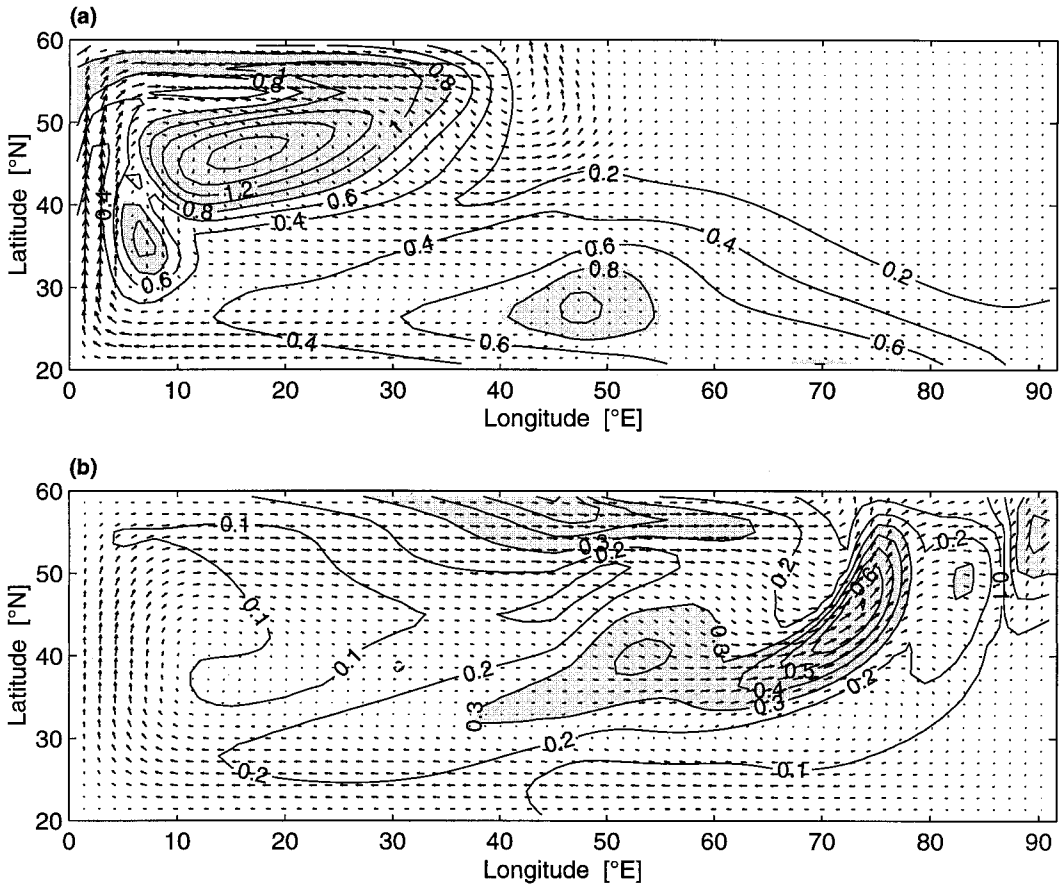

FIG. 5. Same as Fig. 1 but for a basin extended eastward (a) and westward (b) by an equal area with no forcing (expts 74 and 79).

experiment in a channel periodic in the east–west direction. Although similar to one of Winton's experiment, this configuration gives a different result since decadal variability occurs both in PGL and the GFDL MOM code.

b. The eastern boundary

In order to analyze the influence of the eastern boundary, the basin width is doubled through the inclusion of an eastern ''buffer'' zone forced with no surface heat flux (expt 74 for PGL). The consequence of such a change is not dramatic in any model. Figure 5a compares the variability of the surface temperature to the control β plane experiment with Laplacian friction under the zonally uniform ''linear'' surface fluxes. The extrema of the standard deviation of surface temperature are slightly shifted, but the oscillation conserves its initial features. The period lengthens by about 10 yr and the amplitude increases compared to the control run, suggesting that the shorter the distance to the eastern boundary, the more damped the oscillation (in agreement with the enhanced variability observed when the basin width is increased in section 3m). The variability pattern remains almost unchanged in the northwest quarter, is weakest in the southwest quarter, and a new area with significant variability appears in the center of the tropical region. The same conclusions apply when more realistic surface heat fluxes are used (diagnosed from the steady state under restoring boundary conditions for the surface temperature as in expt 81), although the western intensification of these fluxes traps the variability in the western regions and reduces even more the influence of the eastern boundary: the period increases by 5–9 yr, whereas the oscillation index does not significantly change.

c. The polar and tropical boundaries

Following the approach used to examine the role of the eastern boundary, the basin is now extended northward by an equal area with no forcing (expt 75). The characteristics of the β plane are conserved, although it leads to unrealistically large values for the Coriolis parameter in the northern regions (no circulation is expected there anyway). Nevertheless, no fundamental changes occur in the oscillatory behavior or the mean circulation. The period lengthens by more than 10 yr,

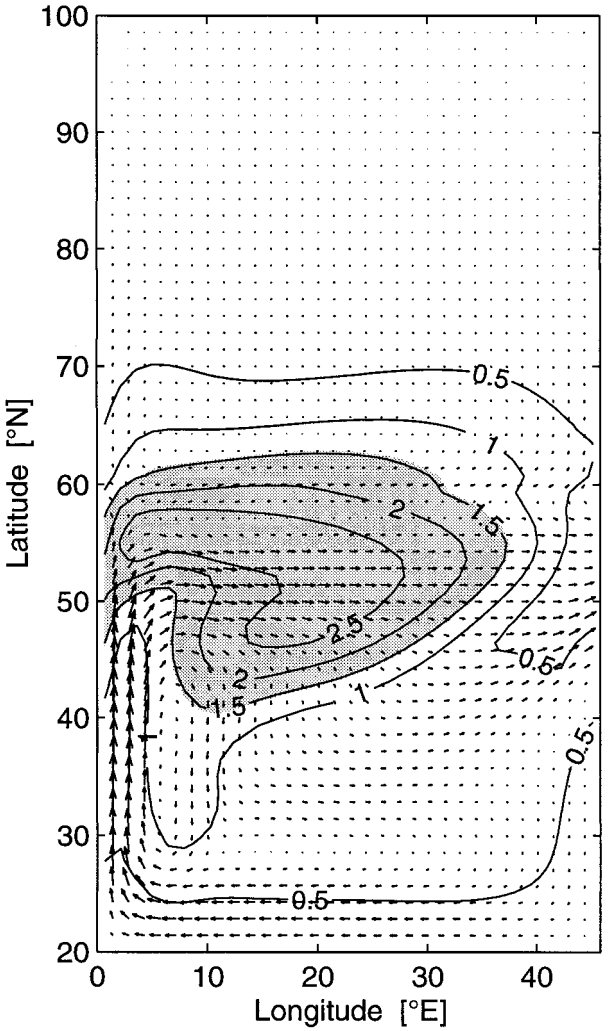

FIG. 6. Same as Fig. 1 but for a basin extended northward by an equal area with no forcing (expt 75).

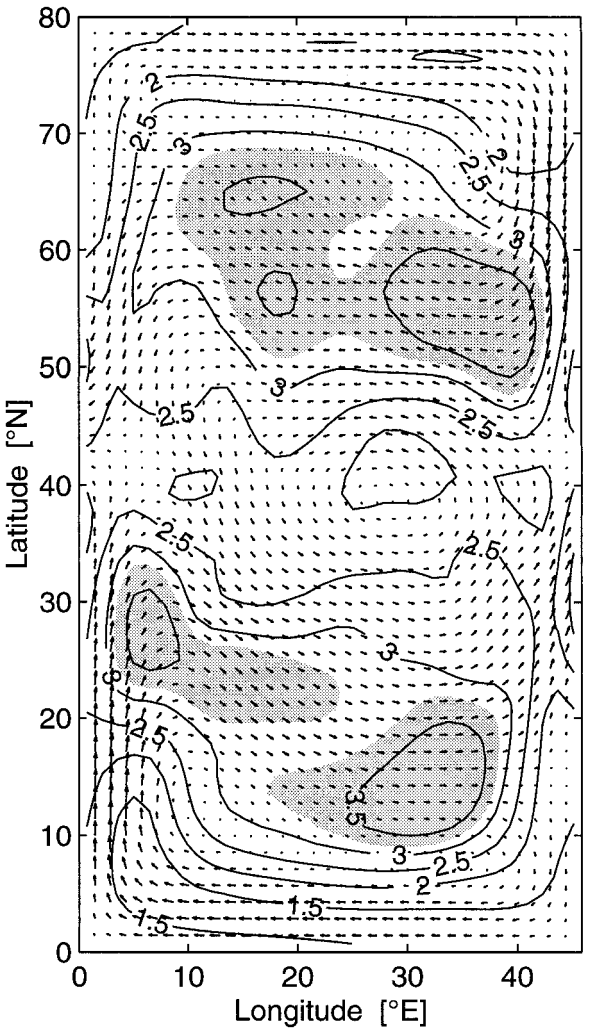

FIG. 7. Same as Fig. 1 but for an f-plane basin extended northward by an equal area, forced by surface heat flux with a cosine profile symmetric relatively to the previous northern boundary (expt 76).

the oscillation amplitude increases, and the variability pattern remains very similar to the standard run, slightly intensified and shifted northward (see Fig. 6). Obviously, the northern boundary plays a weak role in sustaining the oscillations but influences the period. There is no longer a northern boundary to balance pressure gradients in the most variable region (still around 60°N); hence viscous boundary waves cannot explain the variability there. Furthermore, the stratification of the extended area ($N \approx 5 \times 10^{-4}\ \mathrm{s}^{-1}$) induces timescales much shorter than decadal for viscous boundary waves traveling around this region. The variability of the temperature field is also very weak in this area (almost not significant compared to numerical precision). Similar conclusions are obtained using the other models and also with more realistic fluxes diagnosed at the end of the restoring runs (see next section).

The next experiment (expt 76) is set up with the objective to build a thermocline along both southern and northern boundaries: for this purpose, a symmetric surface forcing is applied to the basin with extended northerly domain, but an f plane is chosen in order to keep the Coriolis parameter within a geophysical range. A cosine-dependent surface heat flux profile (full wave, maximum along the northern and southern boundaries and minimum at midlatitude) is used. These experiments produce very intense variability with extreme variations of the regions of convection in every model (see Fig. 7 for PGL). Compared to the standard geometry f-plane experiment forced by a half-wave cosine profile respectively maximum (minimum) at the southern (northern) boundary for the heat flux (expt 77), the oscillation period is longer by 7 yr and the oscillation index doubles. In these cases, we observe a westward propagation of temperature anomalies in the eastward zonal jet. With no zonal boundary in this area, viscous "Kelvin" waves are no longer appropriate and another mechanism must

be found to justify the propagation, recalling that classical Rossby waves are not possible since this experiment considers an f plane. Potential vorticity waves on the mean stratification are a serious alternative since the meridional gradient of potential vorticity is strongly dominated by the meridional temperature gradient.

The role of the tropical boundary is investigated in the same manner as the previous ones, by extending the basin of an equal area southward with no surface forcing, the β plane now spanning from 20°S to 60°N. We do not anticipate a significant dynamical role of this boundary and the numerical simulations (expt 78 for PGL) confirm our expectation: the mean circulation and the oscillations are even more energetic than in the control run.

d. The western boundary

Only the western boundary remains capable of sustaining the oscillations if a boundary is required: GP96, relaxing the temperature field on a very short timescale along each boundary successively, reached this conclusion. W96 suggested that a periodic basin (in the east–west direction) would not produce oscillations, but Marotzke (1990) found decadal variability in the Antarctic Circumpolar Current, suggesting that boundaries may not be crucial. As a first step toward understanding the role of the western boundary, we extend the control basin westward by an equal area with no forcing (expt 79, Fig. 5b). The circulation remains strikingly similar to the control run, although the variability is reduced and shifted eastward from the western boundary current, where the cooling fluxes apply. However, the western boundary current is still there, only displaced westward from the forcing area.

To radically eliminate it, we now consider a channel periodic in the east–west direction: this is not geophysically relevant for the Northern Hemisphere but might apply more realistically to the Antarctic Circumpolar Current. Under the ''linear'' heat flux and in the absence of meridional boundary, the circulation becomes closer to the atmosphere's—that is, principally zonal, and so similar in fact that instabilities develop on the midlatitude thermocline front and generate decadal variability (expt 80). These experiments, implemented both with the GFDL MOM and PGL, suggest that the decadal period is set by the waves that act as perturbations of the mean stratification and circulation. We may speculate that the causes of the variability are similar to those occurring within the atmospheric polar front, that is, baroclinic instability, a point examined in detail in Colin de Verdière and Huck (1999, hereafter CVH).

These results are in contradiction with a previous experiment done by W96: the equations and most parameters (especially horizontal diffusivity) being basically the same, the weaker forcing used by Winton (equivalent to ± 20 W m^{-2} with a half-wave cosine profile) may explain the discrepancy since a sluggish circulation (hence vertical shear) is less likely to develop baroclinic instability (unless details in the coding add to the numerical diffusion, like an upstream vs centered-difference advection scheme).

5. Hints for the mechanism in the transition from steady to oscillatory states

The mechanism invoked by GZ95 and HC94 involving the zonally averaged view of an anomaly of density traveling in the mean circulation and influencing the meridional overturning is rather satisfying in the ideal case of a weakly forced and dissipated system, where anomalies circulate endlessly as in the Howard–Malkus loop (Malkus 1972). However, this is not the case on the decadal timescale, given the large horizontal diffusion used, for instance. Moreover, we will show that the fundamental dynamical link between the overturning and the north–south pressure gradient (inducing a time lag between the two) is necessary for the oscillations to occur. No variability is observed in traditional zonally averaged 2D ocean models forced by constant surface fluxes (W96 and our own experiments). In the experiments of Saravanan and McWilliams (1995), the variability is driven by the high-frequency noise in the atmospheric forcing and integrated by the ocean in interdecadal timescales, and, as such, is based on a very different mechanism. We only develop herein the analysis of the mechanism driving the variability in 3D ocean models forced by constant surface fluxes since a 2D ocean response to stochastic forcing might have different roots.

a. Shift in the mean state when restoring boundary conditions are changed to fixed fluxes

HWC conducted a series of experiments (expts 81 and 85 for PGL on β and f planes) under restoring boundary conditions where the surface temperatures were relaxed to a linear profile varying from 25°C at 20°N to 2°C at 60°N, with a relaxation constant of 35 W m^{-2} K^{-1} (Haney 1971). These experiments ended in steady states within millennia, and we then diagnosed the equivalent surface heat fluxes for each model. We now investigate the evolution of the equilibrium states upon a switch to these fixed-flux boundary conditions. Regular oscillations appear spontaneously in most of the models (expts 82 and 85 for PGL on β and f planes), otherwise a slight perturbation to the temperature field triggers the variability (except for PGRW and PGS). A noticeable deviation from the steady state usually appears within a few hundred years after the shift in boundary conditions, starting as small amplitude oscillations that grow over several oscillations to steady amplitude, as the mean basin stratification adjusts to the cooler bottom waters formed at the surface. The period of the oscillations is almost the same from the first weak

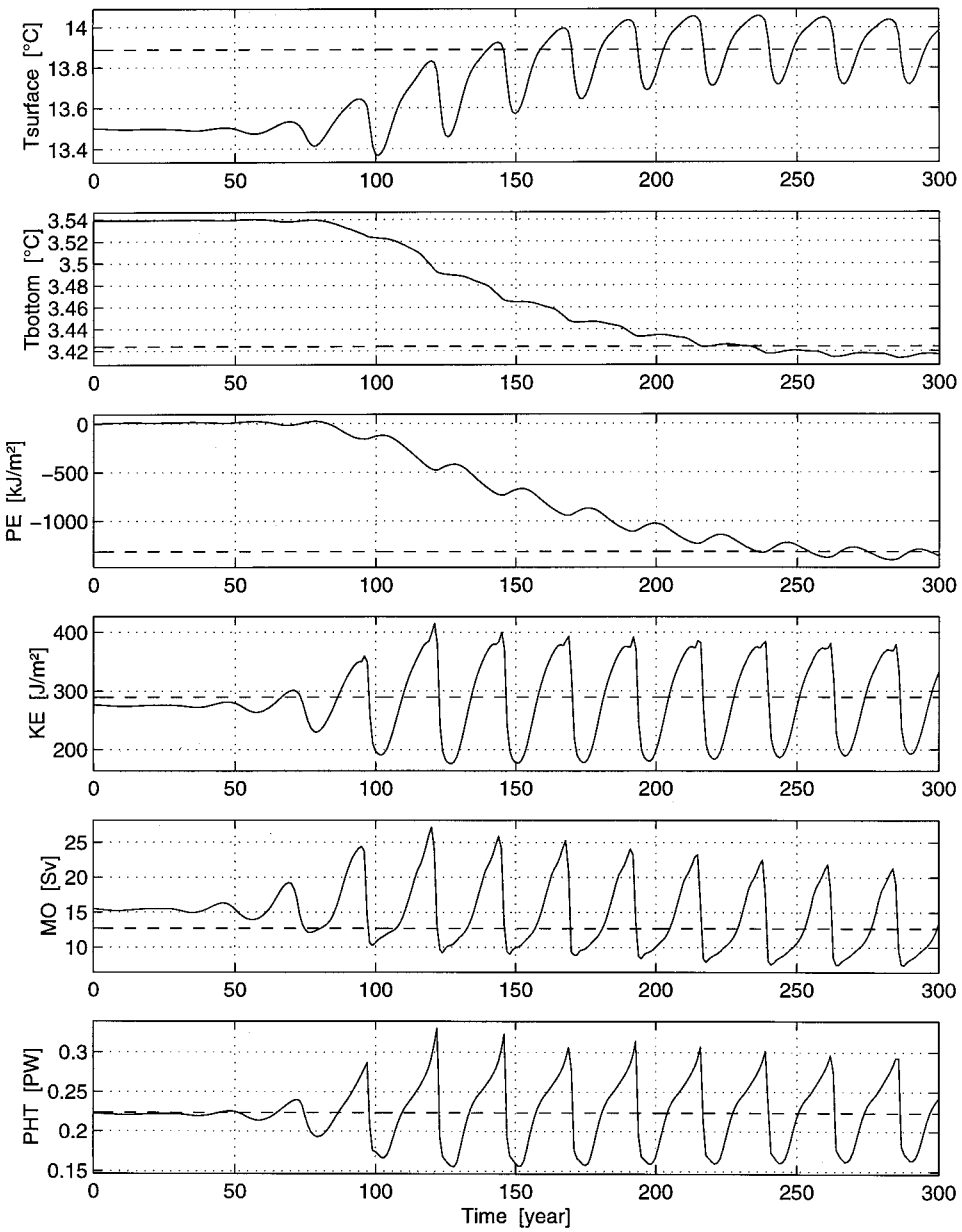

FIG. 8. Transition from the steady state under restoring boundary conditions to the regular oscillations under fixed fluxes diagnosed at the equilibrium of the restoring run (Fig. 10a) for PGL (expt 82): area-averaged surface (0–50 m) and bottom (3950–4500 m) temperatures, potential and kinetic energy density, meridional overturning and maximum advective poleward heat transport as functions of time (after the shift from restoring to diagnosed fixed flux boundary condition).

ones to the final large steady ones (see Fig. 8), suggesting a linear instability mechanism whose period is set by the mean circulation or stratification. These experiments provide a unique opportunity to see how the steady circulation becomes destabilized and evolves into an oscillatory regime. Furthermore, the oscillations are analogous to the ones that settle down within a few thousand years under the same diagnosed fixed fluxes applied to a uniform temperature field (expt 83 for PGL).

The change in the mean state is nearly the same for all the models considered: The mean surface temperature increases along with a decrease in the mean bottom temperature, since cooler minimum temperatures are now achieved at the surface. Potential energy (in its crudest form: $\iiint_V \rho g z \, dV$) thus decreases, whereas kinetic energy slightly increases. However, the time-averaged available potential energy (computed with the method described in HWC) usually slightly increases, thus discarding this stability argument to justify the os-

cillatory state. The time-averaged meridional overturning cell slightly weakens, although the zonal one increases, as well as the potential energy depletion by convection.

b. Change in the variability patterns as a function of the forcing field

Depending on the model, parameters, and forcing, two types of variability appear to take place. The first kind shows a standing temperature anomaly in the northwest region, alternatively positive and negative, as shown in a sequence of snapshots of the upper 250-m temperature and velocity anomalies during an oscillation period for PGL under diagnosed heat fluxes (Fig. 9, expt 82). The second kind, that occurs more often on f planes and under zonally uniform heat flux (expt 3), consists of temperature anomalies traveling westward against the eastward zonal jet in the northern half of the basin. These anomalies induce geostrophically opposite anomalies in their wake by deflecting the mean zonal jet, the main provider of heat in these regions of surface cooling.

Under diagnosed heat fluxes from the restoring runs, we observe an intensification of the variability in the western regions compared to the variability under zonally uniform fluxes used in the parameter sensitivity analysis (Fig. 1 and 10b for PGL on the β plane and Figs. 3 and 11b for PGL on the f plane, but this conclusion applies for the other models as well). These diagnosed fluxes, also strongly intensified in the western regions especially because of the intense cooling above the warm western boundary current, are likely to influence the local stability of the circulation in this area.

c. The regions with maximum anomaly growth rate

To find out where the variability initiates, we analyze the temperature deviations from the equilibrium state after the transition to the diagnosed fixed fluxes (for each model, producing different surface fluxes at the equilibrium under restoring boundary conditions). The extrema of these deviations are usually found at the surface and the maps of surface temperature deviations after a few months look strikingly similar to the maps of surface heat flux where cooling occurs. Namely, most of the extrema for the first months are within one grid point of the maximum of surface cooling, but start to be advected by the mean circulation after a few months. Figures 10 and 11 compare the upper 250-m temperature deviations from the initial equilibrium state to the diagnosed surface heat flux, respectively, in the β- and f-plane cases for PGL (expts 82 and 85). All the models producing variability under diagnosed heat flux similarly show that the seeds of temperature deviation occur in the regions of maximum surface cooling. Since the diagnosed surface fluxes are intimately related to the dynamics through the divergence of the upper layer heat transport, the regions of maximum surface cooling might well be the regions where the vertical profile of velocity is the most likely to be baroclinically unstable: such a question needs more than a paragraph to be properly addressed and is discussed in a later paper (CVH).

Note that the initial temperature deviations are hardly related to the standard deviation of surface temperatures during the regular oscillatory regime. Our interpretation is that after a few decades the instability mechanism shifting the initial state drives the ocean circulation into a resonant mode of the basin such that the oscillation pattern is a consequence of the long baroclinic waves that are periodically excited by the instability mechanism, still providing the necessary source of energy for sustaining the oscillations against dissipation.

The analysis of the maximum temperature deviations during the first years following the shift to fixed-flux boundary conditions suggests that an instability exists in the regions of surface cooling and that the growth rate is maximized where the cooling is the strongest. This result is in agreement with the relation suggested previously between variability patterns and surface heat fluxes. It also recalls more general conclusions drawn within mixed boundary conditions by Weaver et al. (1991) relating decadal variability to the existence of a minimum in the freshwater fluxes. Similarly, Chen and Ghil (1995, 1996) linked the variability to the high-latitude regions where strong evaporation or cooling takes place, in a sector ocean model forced by mixed boundary conditions first, then coupled to an atmospheric energy balance model.

d. A geostrophic amplification of the western anomalies

Snapshots of the anomalous temperature and velocity fields in the transient phase as well as during the fully developed oscillations (Fig. 9) suggest that the immediate geostrophic adjustment of the horizontal circulation usually acts as an amplifier of temperature anomalies developing in the northwestern regions (e.g., due to the previous instability mechanism). Since the western boundary current (WBC hereafter) is the provider of heat in the northern half of the basin, cooled at the surface, its variations imply large temperature deviations. Thus, the heat content of the northwest regions evolves in phase with the WBC transport, as previously noted by GZ95: see also Fig. 13a for the northern half upper temperatures versus Fig. 13e (dashed) for the WBC transport. Since the anomalous temperatures develop a few hundred kilometers off the western boundary (where surface cooling is stronger), the induced geostrophic velocities tend to reinforce the initial WBC deviation.

Furthermore, associated with deviations in the western boundary transport, the upwelling along the western wall in the northern regions is modified. This upwelling, sometimes referred to as the Veronis (1975) effect, has a significant influence on the temperature along the northwest boundary by bringing up cold water from

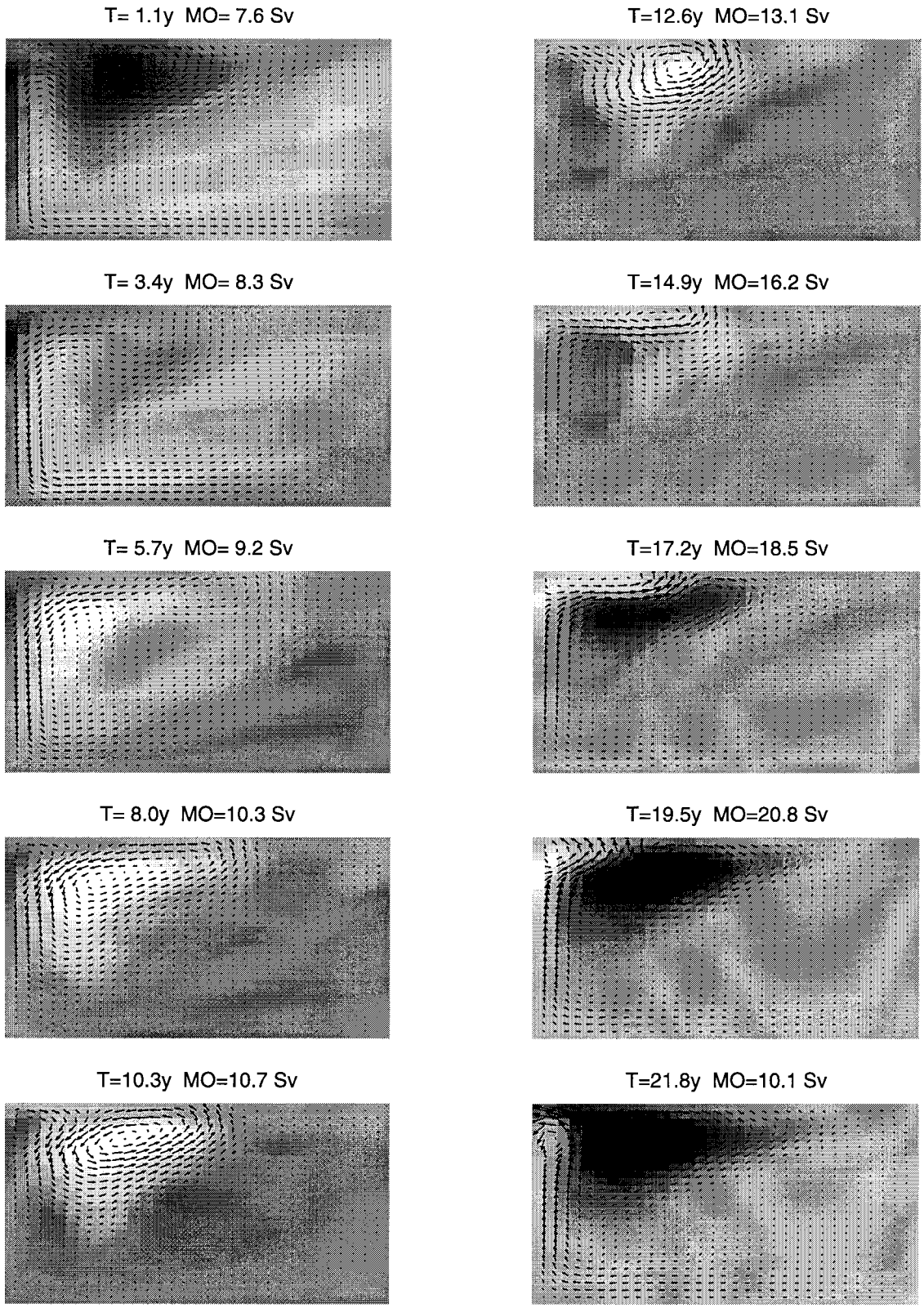

FIG. 9. Snapshots of the anomalies of temperature and velocity in the upper 250 m, in longitude–latitude plane, sampling one oscillation every 2.3 yr of PGL (expt 82) forced by the heat fluxes diagnosed at the equilibrium under restoring boundary conditions (Fig. 10a, expt 81). The scale for velocities is 1 cm s^{-1} per degree. Cold anomalies (<-2°C) are in white while warm anomalies (>2°C) are in black. Abscissa is longitude (0-46°E), ordinate is latitude (20-60°N).

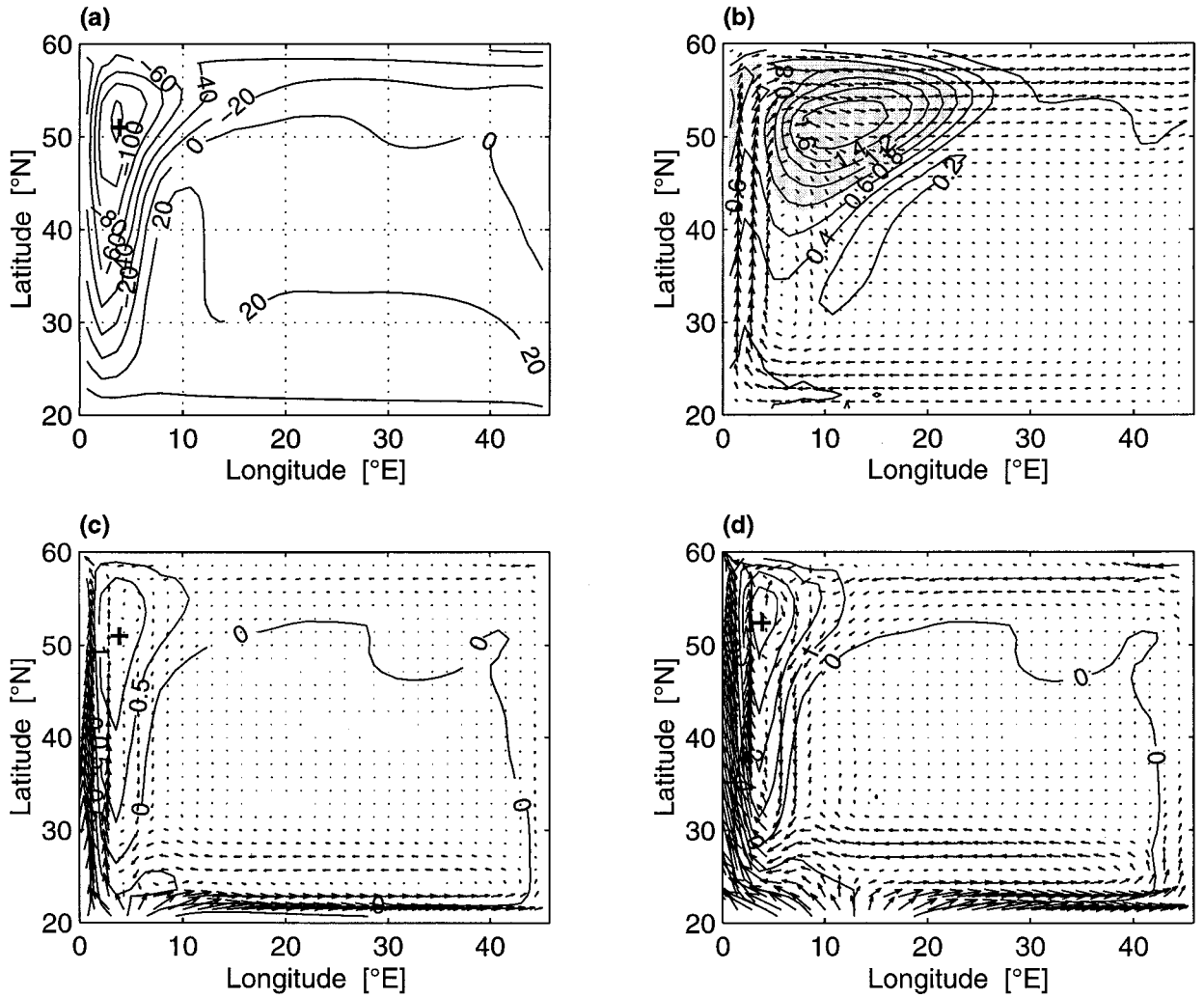

FIG. 10. Transition from restoring boundary conditions to fixed fluxes for PGL on the β plane (expt 82): (a) surface heat fluxes (W m^{-2}) diagnosed at the equilibrium under restoring boundary conditions (expt 81); (b) standard deviation of the upper 250-m temperature (°C) in the regular oscillatory regime; (c) and (d) upper 250-m temperature (10^{-3} °C) and velocity (10^{-4} m s^{-1} per grid spacing) deviations, one and three months after the shift from restoring to diagnosed fixed flux boundary condition. The maximum cooling and deviation regions are shown by a "+."

depth: its role on the whole thermohaline circulation and deep-water properties (Böning et al. 1995; HWC) suggests that it might also play a role in the variability. This upwelling is roughly proportional to the WBC transport and is most active in the northern half: the anomaly it induces along the western boundary is opposite of the one on the east of the WBC (inducing the transport deviation) such that this dipole increases even more the WBC anomaly. Veronis explained this vertical transport of cold water as the only way to balance the artificial cross-isopycnal mixing due to the horizontal diffusion operator across steeply sloping isopycnals in the WBC, but Huang and Yang (1996) argue that it might be an intrinsic feature of the WBC dynamics. However, this process is not necessary for the variability to occur (see section 6 for isopycnal mixing).

Then, different processes interact for the evolution of these temperature anomalies. Geostrophically, because of the mean meridional temperature gradient, a temperature anomaly tends to be advected westward: for example, a warm anomaly induces southward anomalous motion on its east side such that cooler waters are advected in the area, whereas northward motion on its west side brings warmer waters and shifts the anomaly to the west. Such a potential vorticity wave propagation is opposed to the eastward mean flow and, depending on how large and wide the anomaly grows (controlled by diffusion as well), one effect or the other will lead the advection. For instance, under diagnosed heat fluxes intensified to the west (Fig. 9), the anomalies are quite stationary in the northwest corner; whereas in the control run under zonally uniform heat flux, large anomalies

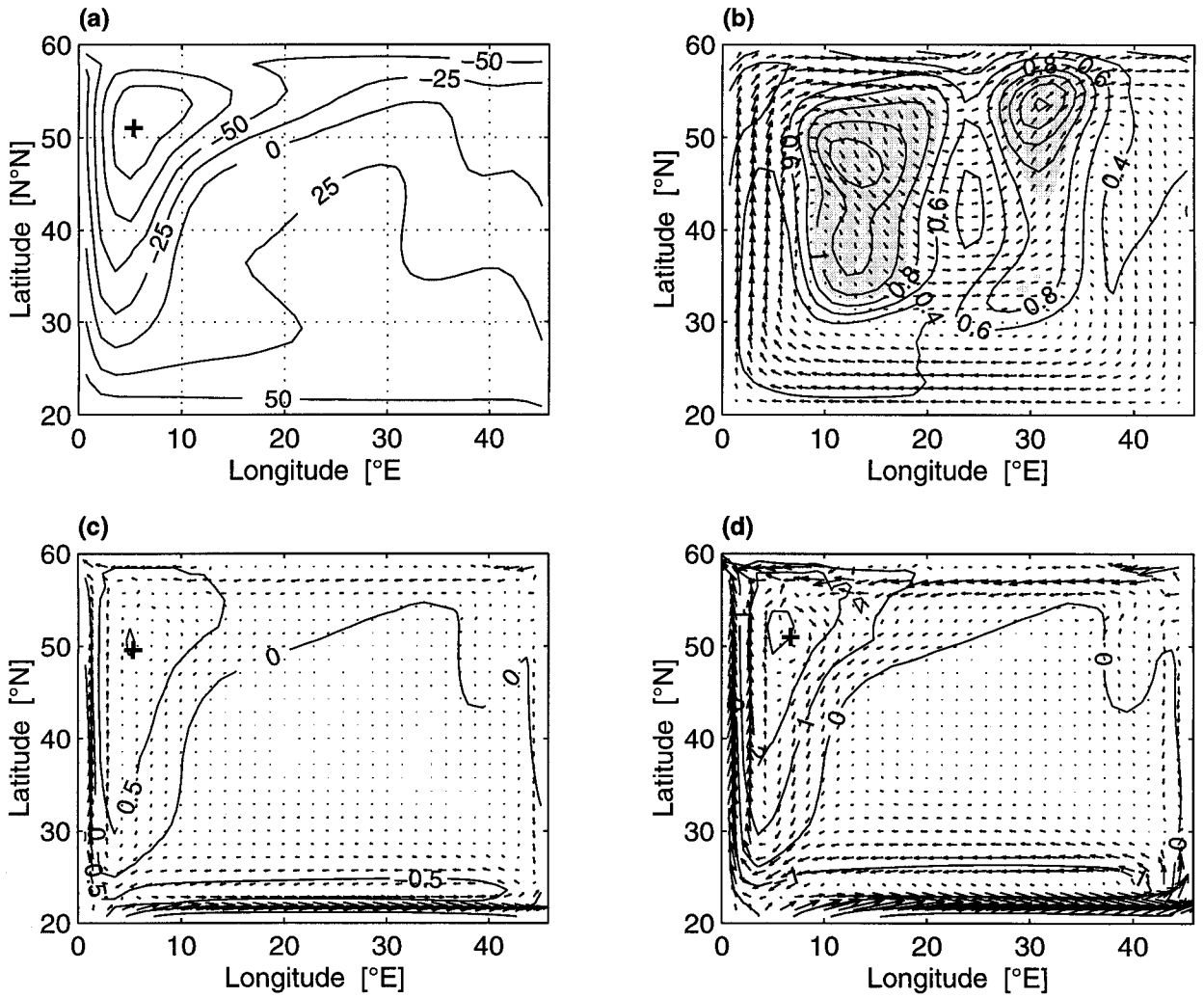

FIG. 11. Same as Fig. 10 but on the f plane (expts 84 and 85).

move clockwise across the basin as small opposite anomalies propagate westward along the northern boundary. In addition to the propagation mechanism, given the northern region heat balance between eastward advection of heat and surface cooling, an anomaly deflects the eastward zonal jet in its wake such that an opposite anomaly grows there. When the initial anomaly is trapped along the western boundary, the opposite one induced on its east side keeps intensifying and, once large enough, propagates westward and reverses the western boundary current anomaly.

e. The meridional overturning adjustment to the density anomalies

Of course, the geostrophic amplification mechanism previously described cannot hold for long since it builds its own destruction. On longer timescales, a growing warm anomaly in the northwest quarter, increasing the WBC transport, finally reduces the north–south density gradient and modifies the global overturning. However, the adjustment of the meridional cell to the density structure implies geostrophic (long baroclinic Rossby waves and potential vorticity waves) and boundary waves, whose consequences and associated timescales are not easily predictable. Therefore, we further use an indirect method in order to relate the oscillation period to this adjustment process.

The analysis of the response of the thermohaline circulation to small perturbations introduced through the salinity field in the northern regions enlightens the adjustment mechanism. At equilibrium under restoring boundary conditions for surface temperature (salinity uniformly set to 35 psu and not forced: expt 81 for PGL), we introduce a 0.05 psu salinity anomaly in the upper 150 m of the region between 50° and 60°N over the longitudinally centered third of the basin. Salinity is used rather than temperature because it does not directly change the surface fluxes under restoring boundary conditions and allows us to differentiate the introduced per-

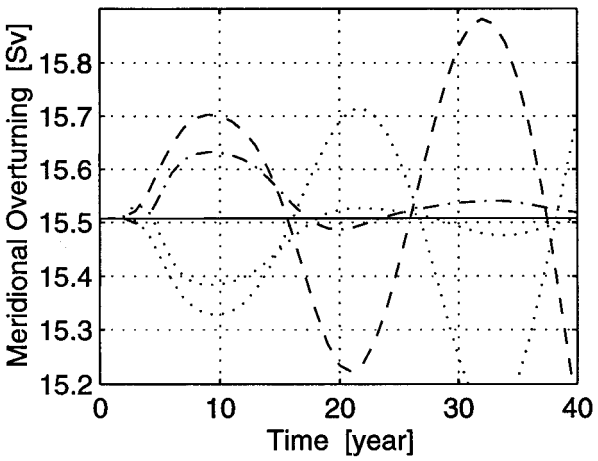

FIG. 12. Meridional overturning (Sv) as a function of time under restoring boundary conditions (dash–dotted) vs fixed heat fluxes diagnosed from the equilibrium of the restoring run (dashed), after the introduction of a 0.05 psu salinity anomaly in the centered north of the basin. The responses to the opposite anomaly are plotted as well (dotted). The initial state is the equilibrium state under restoring boundary conditions. The regular oscillations regime under diagnosed heat fluxes has a period of 23 yr, very similar to the initial cycles period. Note the damping effect of the restoring boundary conditions on temperature anomalies, compared to the amplification under fixed fluxes.

turbation from the dynamically induced one. A linear equation of state relates the density anomaly to the temperature ($\alpha = 2 \times 10^{-4}$ K^{-1}) and to the salinity ($\beta = 8 \times 10^{-4}$ psu^{-1}). Then, we compare the adjustment of the equilibrium state to the weak salinity anomaly under the restoring boundary conditions and the associated diagnosed fixed-flux boundary conditions. These experiments show a similarity in the response during the first years, but a different evolution of the perturbations afterward (Fig. 12 for PGL): The anomalous temperatures are damped out within a few cycles under restoring boundary conditions, whereas they amplify under fixed fluxes and reach the full amplitude of the oscillatory state within a few hundred years, the time for the mean basin temperature to adjust as well. Except in PGRW, we observe an overshoot of the meridional overturning in response to the perturbation under both boundary conditions. These experiments suggest mainly that the period of the oscillations is set by the mean stratification and circulation independently of the perturbation amplitude or the boundary conditions: even the infinitesimal first cycles on Fig. 12 show the same period as the fully developed oscillations, implying that the temperature anomaly amplitude does not influence their dynamics. This is noteworthy since most of the regular oscillations induce large changes in the upper temperature and circulation such that nonlinear interactions might be expected as compared to the small perturbation experiment done here. Temperature anomalies associated with geostrophic circulation anomalies are seen traveling westward against the eastward zonal jet in the northern part of the basin, crossing the basin within a few years before reaching the western boundary current: this looks more like geostrophic (potential vorticity) waves than viscous boundary waves since there is no intensification close to the coast. This behavior is observed in f plane simulations as well; therefore, these are not classical baroclinic Rossby waves (based on the β effect). As pointed out earlier, the meridional variations of potential vorticity in the upper layers are dominated by the meridional temperature gradient (forced by the differential heating), and the variations of the Coriolis parameter become significant only in the deeper layers where the stratification and the meridional gradients are weak. This implies, incidentally, that the meridional gradient of potential vorticity changes sign in the vertical over most of the ocean domain, a necessary condition for baroclinic instability. Furthermore, the surface-intensified waves mainly feel the meridional gradient set by the temperature contrasts. These potential vorticity waves on the mean stratification (function of latitude) and circulation (eastward zonal jet) provide a potential explanation for the decadal timescale and for shaping up the oscillation pattern.

f. A simple box-model analogy for the oscillation

Drastically reducing the degrees of freedom of ocean models has proved successful in the past for the understanding of multiple equilibria of the thermohaline circulation, for instance (Stommel 1961). Box models are the most simple architecture to investigate process studies, and we try in the following to brush a picture of the decadal oscillation in such an idealized formalism. The analysis of these oscillations in terms of zonal averages is complicated by the phase shift of temperature deviations along the same latitude circle such that zonally averaged temperatures vary much less than expected from local deviations. Thus, the definition of mean temperature for the traditional polar (T_1) and tropical (T_2) boxes in these models filters most of the variability. However, it allows us to look at the correlation between meridional overturning (O) and north–south density gradients (proportional to $\Delta T = T_2 - T_1$). We define a polar and a tropical box of equal size, separated by the 40°N parallel and 400-m deep. In Fig. 13, we plot the time evolution of the mean temperatures in these boxes along with their difference, the meridional overturning, the WBC transport in the upper 400 m, and their time derivatives, for the low-resolution run under linear heat flux (expt 49). In contrast with what is usually stated in box and zonally averaged ocean models (Stommel 1961), meridional overturning anomalies and north–south density gradient anomalies are closer to quadrature (correlation coefficient ≈ 0.95) than in phase ($r \approx -0.03$). Other models give similar results although the time evolution of the meridional overturning is less sinusoidal at higher resolution (see Fig. 8 vs 13). This confirms that on decadal timescales, the adjustment pro-

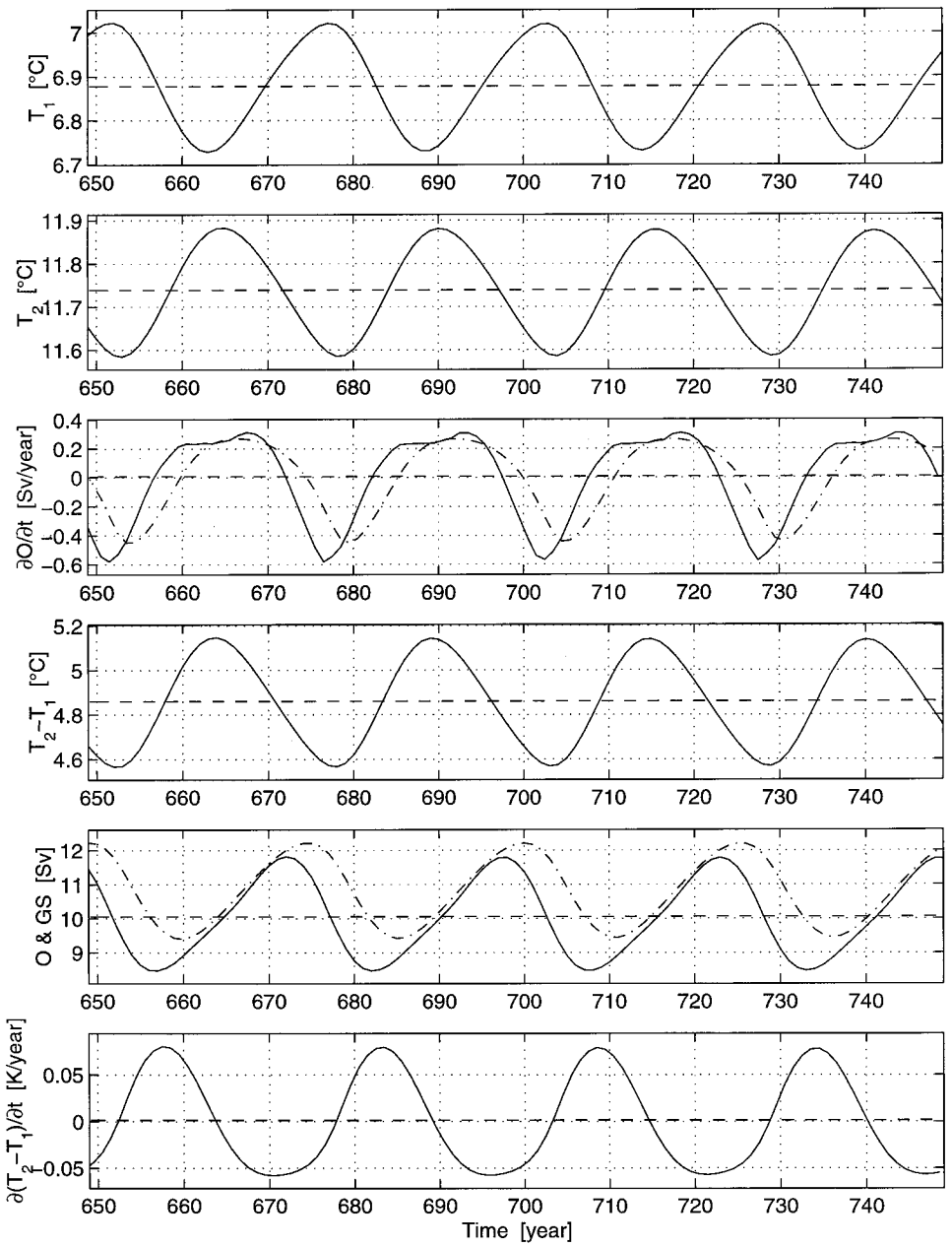

FIG. 13. Mean temperature in the upper 400 m for the north (T_1) and south (T_2) halves of the basin (°C) and difference, western boundary current transport in the upper 400 m (GS, dash–dotted) and maximum of the meridional overturning streamfunction (O, in Sv), $\partial(T_2 - T_1)/\partial t$ [K yr^{-1}], $\partial O/\partial t$ [Sv yr^{-1}] as functions of time during a few oscillations in the low resolution PGL run forced by the "linear" heat flux (expt 49). The linear regression coefficient is 1.38 (1.0) Sv yr^{-1} K^{-1} between $\partial O/\partial t$ (∂GS/∂t) and $T_2 - T_1$, with a correlation coefficient of 0.92 (0.80), whereas it is -0.04 K yr^{-1} Sv^{-1} between $\partial(T_2 - T_1)/\partial t$ and O or GS, with correlation coefficients of respectively, -0.97 and -0.79. The slow growth but fast breakdown of the meridional overturning seen at higher resolution (Fig. 8) is avoided here, thanks to the low resolution.

cess cannot be neglected since the equilibrium overturning is never reached.

Consequently, a simple box-model analogy representing the decadal oscillations is formulated as follows, with a parameterization of the adjustment process such that the time derivative of the meridional overturning is linearly related to the north–south density gradient anomaly. We consider a thermocline box (volume: $V \approx$ 2000 km $\times$ 4000 km $\times$ 400 m, temperature: $T \approx 12$°C), warmed by a constant heat flux ($A \times Q_H$: $A \approx$ 2000 km $\times$ 4000 km, $Q_H \approx 35$ W m^{-2}), and a cold box (volume: $V_0 \gg V$, temperature: $T_0 \approx 5$°C) including the

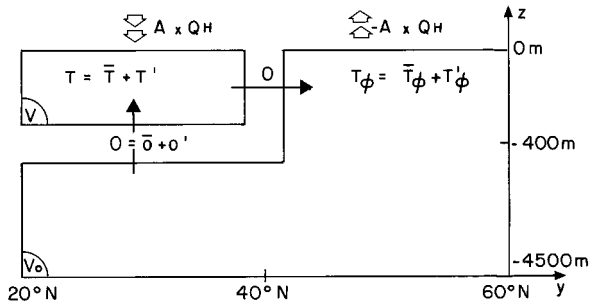

FIG. 14. A simple box model for the oscillation.

polar and deep waters, cooled by the opposite heat flux, such that the mean basin temperature remains constant (Fig. 14). The mass exchange ($O \approx 10$ Sv) between these boxes represents the traditional overturning cell, moving thermocline waters poleward through the western boundary current, balanced by upwelling across the base of the thermocline (in the interior and/or along the western boundary). Thus, the equations controlling the temperature of the boxes are

$$\rho_0 C_P V \frac{\partial T}{\partial t} = +AQ_H + \rho_0 C_P O(T_0 - T)$$

$$\rho_0 C_P V_0 \frac{\partial T_0}{\partial t} = -AQ_H + \rho_0 C_P O(T - T_0).$$

Decomposing T, T_0, and O in a time average and deviation, noted by an overbar and a prime, respectively, the time-averaged equations become

$$\rho_0 C_P \overline{O}(\overline{T} - \overline{T}_0) = AQ_H,$$

whereas the first-order linearization for the deviation from the time average gives

$$\frac{\partial T'}{\partial t} = -\frac{O'}{V}(\overline{T} - \overline{T_0}) - \frac{\overline{O}}{V}(T' - T'_0)$$

$$= -O'\frac{\overline{T} - \overline{T_0}}{V} - T'\overline{O}\left(\frac{1}{V} + \frac{1}{V_0}\right), \qquad \text{(E1)}$$

recalling that the mean basin temperature is constant: $VT' + V_0 T'_0 = 0$. From the previous paragraph, the rate of change of the overturning deviation is chosen proportional to the south–north temperature anomaly gradient to parameterize crudely the time lag between anomalous pressure anomalies and overturning adjustment (the proportionality constant k is found around 1 Sv yr^{-1} K^{-1} in most of the numerical experiments):

$$\frac{\partial O'}{\partial t} = k(T' - T'_0) = T'k\left(1 + \frac{V}{V_0}\right). \qquad \text{(E2)}$$

In a first approximation mostly verified in the experiments forced by diagnosed heat flux (Fig. 8), we suppose that $|O'/\overline{O}| \gg |T'/(\overline{T} - \overline{T}_0)|$ (this is barely achieved in Fig. 13 by a factor of 3) such that the second term in the right-hand side of (E1) can be neglected. Then, the time evolution of T' is simply sinusoidal with period $2\pi[k(\overline{T} - \overline{T}_0)(1/V + 1/V_0)]^{-1/2} \approx 23$ yr, with $\overline{T} - \overline{T}_0 = 7$°C. However, when solving the full system (E1, E2), the previously neglected term in (E1) leads to an e-folding timescale similar to the period: $\tau = 2[\overline{O}(1/V + 1/V_0)]^{-1} \approx 19$ yr. Obviously, we lack a driving term representing the instability process that supplies energy to the perturbation during each period to sustain the oscillations: the possibility of baroclinic instability as a potential candidate has been alluded to in the past on theoretical grounds (Colin de Verdière 1986), but has yet to be recognized as an important source of large-scale variability in coarse oceanic GCMs—this is the subject of CVH. Nevertheless, this simple model illustrates how crucial for the oscillation is the time lag between the overturning and the north–south density gradient, through the westward propagation of various waves (geostrophic, Rossby, PV, or viscous boundary) across the basin. If O' is taken in phase with $(T' - T'_0)$, no periodic solution can be found. Finally, the parameterization makes sense if one imagines the thermohaline cell forced by differential gravity forces, like in the Welander's circulation tube of Malkus (1972) where the rate of change of the transport is related to the torque of the weight applied to the nonuniform fluid density.

6. Robustness of the variability to various parameterizations and forcing

The range of forcing leading to variability in the literature suggests that at least one variable of the density equation requires more freedom than allowed by the usual short timescales used in restoring boundary conditions. Applying the idea of Schopf (1983), we reduce the implicit infinite heat capacity of the atmosphere assumed in strong restoring boundary conditions by reducing the relaxation constant (lengthening the restoring timescale). At the same time the specified atmospheric temperature amplitude is increased such that the thermohaline circulation keeps a reasonable intensity. GZ95 carried out similar experiments that resulted in decadal oscillations. With the same parameters as the control run described in section 2, we carried out experiments (expt 86 for PGL) with restoring temperatures varying from 29°C at 20°N to −2°C at 60°N and a relaxation constant of 10 W m^{-2} K^{-1}, as suggested by Seager et al. (1995) from simple thermodynamic models of the lower atmosphere: Regular decadal oscillations were sustained for thousands of years with amplitude and periods similar to the control run. The standard deviation of the upper 250-m temperature is shown in Fig. 15 and looks very similar to previous variability patterns. The time-averaged surface fluxes vary between −50 W m^{-2} in the northwest corner to 30 W m^{-2} along the tropical boundary. We also obtained variability under restoring boundary conditions with traditional relaxation constant (35 W m^{-2} K^{-1}) when using increased vertical mixing

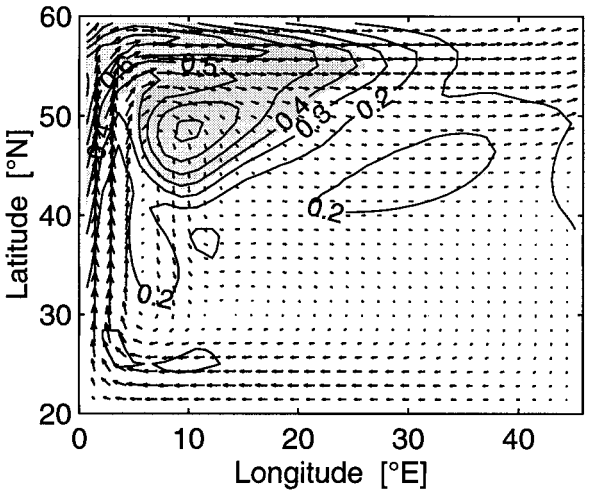

FIG. 15. Same as Fig. 1 for PGL, under restoring boundary conditions for the surface temperatures to a linear profile varying from 29°C at 20°N to −2°C at 60°N, with a 10 W m^{-2} K^{-1} relaxation constant.

for tracer ($\geq 5 \times 10^{-4}$ m^2 s^{-1}) in the MOM (but not with the planetary geostrophic models): the intensity of the meridional overturning is then strong enough (>25 Sv) and decadal oscillations occur spontaneously. Although in this case the surface damping of anomalies does not vary, it is the amplitude of the overturning (through stronger instabilities of the western boundary current or the eastward zonal jet) that triggers the oscillations.

The potential role of the upwelling along the western boundary in sustaining the oscillation is invoked in the description of the geostrophic processes amplifying temperature anomalies (section 5d). This is also supported by the reluctance of PGRW (where vertical velocities are reduced along the boundaries by allowing horizontal recirculations in tangential velocities along the coasts) to sustain variability under fixed fluxes diagnosed at equilibrium under restoring boundary conditions (also if horizontal diffusion is increased to 1000 m^2 s^{-1} under "linear" heat fluxes, PGRW is the only one to remain in a steady state). To investigate the sensitivity of the oscillatory behavior to diapycnal mixing (through cross-isopycnal vertical velocities along the boundaries), we compare various experiments with the GFDL MOM. The geometry, parameters, and forcing remain the same as in the control run except that now the mixing tensor is rotated along isopycnal coordinates (the background vertical diffusivity was not changed from the control run). The oscillations prove robust to this parameterization (expt 87): the period becomes irregular (around 20 yr) while the amplitude of KE variations increases. We then include the Gent and McWilliams (1990) parameterization for mesoscale eddy-induced tracer transport (expt 88): The amplitude of the oscillation is now reduced and the period shortened (16 yr instead of 25), but the variability is still sustained with patterns similar to the control run. The same conclusions apply when this parameterization is used along with horizontal mixing (expt 89).

The addition of a steady wind stress, forcing a barotropic streamfunction that interacts nonlinearly with the thermohaline circulation, is also carried out [expt 90 for PGL with the analytical wind stress of Bryan (1987)]. Various profiles of zonally uniform zonal wind stress are tested, inducing one or two gyres in the standard flat-bottomed basin. In all cases, the oscillations survive, with shifts in the variability patterns and changes in the period and amplitude. It seems that the interaction with the wind-forced circulation, as implemented here, does not influence the mechanism driving the decadal variability of the thermohaline cell. However, recent experiments with reduced vertical mixing suggest that the amplitude of the wind forcing may significantly affect the period.

Finally, we introduce seasonal variations in the forcing field (similar to the North Atlantic annual cycle for the zonal-mean net downward heat flux) to test the robustness of the decadal variability to continuously varying forcing and circulation (expt 91 for PGL). This has no significant effect on the oscillation, although the linear equation of state, the lack of wind stress, and freshwater forcing (and their seasonal variations) might contribute to these limited changes. The seasonal cycle, whose amplitude remains smaller than the decadal one, seems not to interact at all with the longer scales of decadal oscillations.

7. Conclusions

We have analyzed interdecadal oscillations of the thermohaline circulation arising under fixed surface fluxes (or restoring boundary conditions with realistically long restoring timescales) in box-geometry ocean basins, with planetary geostrophic and primitive equations models at coarse resolution (160 km). Through a systematic comparison of the results from several models with different parameterizations of momentum dissipation and associated boundary conditions, an extensive parameter sensitivity analysis enables us to determine which processes are critical to the variability. Use of spherical or Cartesian coordinates, as well as the variation of β with latitude or a constant midlatitude value, were shown to have no crucial influence on the oscillations. However, f-plane experiments suggested a leading role of the geostrophic balance since increasing the Coriolis parameter increases the oscillation amplitude and period although it weakens the mean circulation. Furthermore, a nonrotating experiment, although highly energetic, induced no variability. Vertical diffusion has a driving role on the variability (certainly through its influence on the meridional overturning), while horizontal diffusion has a crucial damping role. Within the range of uncertainty in the actual ocean mixing, the variability is sustained in all of the models or

in none. A numerical scheme relating the horizontal mixing to local velocities, as well as isopycnal mixing with or without the eddy-induced tracer transport parameterization of Gent and McWilliams (1990), does not profoundly influence the oscillatory behavior. Convective adjustment, well-known to produce grid-scale noise and influence the stability of the thermohaline circulation, is not necessary to sustain these oscillations (only for the removal of static instabilities). Momentum dissipation parameterizations and associated boundary conditions have a significant influence on the oscillation period and amplitude, although they only modify the velocities along the boundaries but not the geostrophic balance in the interior. Nevertheless, the variability is reproduced in all these models. The friction coefficients have a damping effect on the oscillations, in agreement with the driving role of the Coriolis parameter. Horizontal and vertical resolutions are not fundamental but may modify the variability if not fine enough: the variability also occurs more easily at higher resolution. Thus, interdecadal oscillations stand out as a robust geostrophic feature of thermohaline circulation models forced by constant surface fluxes in idealized geometry, but their amplitude and period is controlled by parameterized subgrid-scale diffusion processes.

We further investigated the role of the boundaries and the propagation of viscous boundary waves, as proposed in previous studies. Our results suggest that the propagation of boundary waves along a weakly stratified boundary does not capture the overall processes that explain the characteristics and timescales of the oscillations. The intensification of the standard deviation of the upper-layer temperature in the northwest quarter of the basin, in the eastward zonal jet continuing the western boundary current where surface cooling is the strongest, suggests instability processes in this area (the relevance of baroclinic instability is thoroughly analyzed in CVH).

We finally provide hints for the driving mechanism in the analysis of the transition between a steady state (under restoring boundary conditions) and an oscillatory regime under the fixed fluxes diagnosed at equilibrium of the restoring run. The time-averaged state varies between the two regimes, since cooler deep water is formed during the oscillations (the potential energy, but not the available potential energy, is lower in the final state). The initial deviations from the steady state appears in the regions of strongest surface cooling, where a purely geostrophic amplification mechanism of temperature anomalies in the vicinity of the western boundary takes place. The oscillation period is related to the meridional overturning adjustment to density anomalies. Finally, a simple box model is proposed that captures the phase shift between the meridional overturning anomalies and anomalous north–south temperature gradients and reproduces the oscillatory behavior and period.

Even if these oscillations might not apply to the real ocean because of the damping of baroclinic modes by bottom pressure torque with realistic topography (Winton 1997; Greatbatch et al. 1997, manuscript submitted to *J. Geophys. Res.*), understanding the variability in simple configurations is a first step in addressing more complex and realistic scenarios.

Acknowledgments. This research was funded through a scholarship awarded to TH from the French Ministry of Education and strategic and operating grants awarded to AJW from NSERC, CICS, and the NOAA Scripps–Lamont Consortium on the Ocean's Role in Climate. Thanks to a particular reviewer, additional experiments along with the revision process, funded through Grant NSF ATM 9710285 awarded to Geoffrey K. Vallis (supporting TH), helped clarify the conclusions.

APPENDIX

Geostrophic Scaling of the Overturning Streamfunction under Constant Flux Boundary Condition

Huang and Chou (1994) developed a geostrophic scaling for the ocean circulation driven by constant freshwater flux, applied by Weaver and Garrett[1] to the buoyancy flux. We briefly recall this scaling to allow a comparison with the numerical experiments. Let U and V be characteristic horizontal geostrophic scales, W a characteristic vertical velocity; D a characteristic thermocline depth scale; L_X and L_Y the zonal and latitudinal scales of the ocean basin, f the Coriolis parameter; b_X and b_Y characteristic buoyancy contrasts in each direction (a priori different), and B the characteristic surface buoyancy flux. From hydrostatic and geostrophic balances, the thermal wind equation gives

$$\frac{fU}{D} = \frac{b_Y}{L_Y} \quad \text{or} \quad \frac{fV}{D} = \frac{b_X}{L_X}.$$

The continuity equation relates U, V, and W through the typical length scales:

$$\frac{U}{L_X} = \frac{V}{L_Y} = \frac{W}{D}.$$

Given a constant vertical diffusivity K_V, the Munk balance for the vertical advective–diffusive tracer equilibrium across the thermocline imposes $K_V = WD$. Then, the density gradient can be related to the surface fluxes via the boundary condition:

$$K_V \frac{\partial b}{\partial z} = B, \quad \text{that is,} \quad K_V \frac{b}{D} = B,$$

and via the horizontal tracer advection in the thermocline:

[1] Unpublished manuscript on the sensitivity of the thermohaline circulation in an OGCM to vertical eddy diffusivity.

TABLE A1. Power law for the dependency of the meridional overturning on various parameters.

Parameter	Range	Scaling	PGL	PG0	PGR0	PGRW	Mean
f on f plane	$[2\Omega\sin(14°)-2\Omega\sin(66°)]$	−1/4	−0.60	−0.35	−0.57	−1.07	−0.65
f on β plane	$[2\Omega\sin(26°)-2\Omega\sin(90°)]$	−1/4	−0.32	−0.27	−0.22	−0.60	−0.35
K_v	$(10^{-5}$–10^{-3} m^2 s^{-1})	1/2	0.37	0.46	0.41	0.45	0.42
B	(5–135 W m^{-2})	1/4	0.22	0.32	0.17	0.22	0.23
L_x	(2560–10 240 km)	3/4	0.69	0.60	0.73	0.85	0.72

$$DU\frac{b_X}{L_X} = DV\frac{b_Y}{L_Y} = B,$$

which shows that $b_X = b_Y = b$. Thus, the thermocline depth and the meridional overturning can be deduced from the parameters:

$$D = \left(\frac{K_V^2 L_X L_Y f}{B}\right)^{1/4},$$

$$\Psi = UDL_Y = VDL_X = WL_X L_Y = \left(\frac{K_V^2 L_X^3 L_Y^3 B}{f}\right)^{1/4}.$$

Table A1 gives the regression coefficients of Ψ function of each parameter in log–log coordinates for the numerical experiments with various models. Most of these values match reasonably the scaling except for the Coriolis parameter on f planes, a rather disturbing result since the geostrophic equations are precisely the basis for the scaling. The β-plane dynamics agree better with the scaling, although it is not explicit in the scaling.

REFERENCES

Anderson, D., and A. E. Gill, 1975: Spin-up of a stratified ocean, with applications to upwelling. *Deep-Sea Res.,* **22,** 583–596.

Armi, L., and H. Stommel, 1983: Four views of a portion of the North Atlantic subtropical gyre. *J. Phys. Oceanogr.,* **13,** 828–857.

Böning, C. W., W. R. Holland, F. O. Bryan, G. Danabasoglu, and J. C. McWilliams, 1995: An overlooked problem in model simulations of the thermohaline circulation and heat transport in the Atlantic Ocean. *J. Climate,* **8,** 515–523.

Bryan, F., 1987: Parameter sensitivity of primitive equation ocean general circulation models. *J. Phys. Oceanogr.,* **17,** 970–985.

Bryan, K., S. Manabe, and R. C. Pacanowski, 1975: A global ocean–atmosphere climate model. Part II: The oceanic circulation. *J. Phys. Oceanogr.,* **5,** 30–46.

Cai, W., R. J. Greatbatch, and S. Zhang, 1995: Interdecadal variability in an ocean model driven by a small, zonal redistribution of the surface buoyancy flux. *J. Phys. Oceanogr.,* **25,** 1998–2010.

Capotondi, A., and R. Saravanan, 1996: Sensitivity of the thermohaline circulation to surface buoyancy forcing in a two-dimensional ocean model. *J. Phys. Oceanogr.,* **26,** 1039–1058.

Cessi, P., 1996: Grid-scale instability of convective-adjustment schemes. *J. Mar. Res.,* **54,** 407–420.

Chen, F., and M. Ghil, 1995: Interdecadal variability of the thermohaline circulation and high-latitude surface fluxes. *J. Phys. Oceanogr.,* **25,** 2547–2568.

——, and ——, 1996: Interdecadal variability in a hybrid coupled ocean–atmosphere model. *J. Phys. Oceanogr.,* **26,** 1561–1578.

Colin de Verdière, A., 1986: On mean flow instabilities within planetary geostrophic equations. *J. Phys. Oceanogr.,* **16,** 1981–1984.

——, 1988: Buoyancy driven planetary flows. *J. Mar. Res.,* **46,** 215–265.

——, 1989: On the interaction of wind and buoyancy driven gyres. *J. Mar. Res.,* **47,** 595–633.

——, and T. Huck, 1999: Baroclinic instability: An oceanic wavemaker for interdecadal variability. *J. Phys. Oceanogr.,* **29,** 893–910.

Delworth, T., S. Manabe, and R. J. Stouffer, 1993: Interdecadal variations of the thermohaline circulation in a coupled ocean–atmosphere model. *J. Climate,* **6,** 1993–2011.

Deser, C., and M. L. Blackmon, 1993: Surface climate variations over the North Atlantic Ocean during winter: 1900–1989. *J. Climate,* **6,** 1743–1753.

Fanning, A. F., and A. J. Weaver, 1998: Thermohaline variability: The effects of horizontal resolution and diffusion. *J. Climate,* **11,** 709–715.

Frankignoul, C., P. Müller, and E. Zorita, 1997: A simple model of the decadal response of the ocean to stochastic wind forcing. *J. Phys. Oceanogr.,* **27,** 1533–1546.

Freeland, H., P. Rhines, and T. Rossby, 1975: Statistical observations of the trajectories of neutrally buoyant floats in the North Atlantic. *J. Mar. Res.,* **33,** 383–404.

Gent, P. R., and J. C. McWilliams, 1990: Isopycnal mixing in ocean circulation models. *J. Phys. Oceanogr.,* **20,** 150–155.

Greatbatch, R. J., and S. Zhang, 1995: An interdecadal oscillation in an idealized ocean basin forced by constant heat flux. *J. Climate,* **8,** 81–91.

——, and K. A. Peterson, 1996: Interdecadal variability and oceanic thermohaline adjustment. *J. Geophys. Res. [Oceans],* **101,** 20 467–20 482.

Griffies, S. M., and K. Bryan, 1997: Predictability of North Atlantic multidecadal climate variability. *Science,* **275,** 181–184.

Haney, R., 1971: Surface thermal boundary condition for ocean circulation models. *J. Phys. Oceanogr.,* **1,** 241–248.

Hansen, D. V., and H. F. Bezdek, 1996: On the nature of decadal anomalies in North Atlantic sea surface temperature. *J. Geophys. Res.,* **101,** 8749–8758.

Hasselmann, K., 1982: An ocean model for climate variability studies. *Progress in Oceanography,* Vol. 11, Pergamon, 69–92.

Huang, R. X., 1993: Real freshwater flux as a natural boundary condition for the salinity balance and thermohaline circulation forced by evaporation and precipitation. *J. Phys. Oceanogr.,* **23,** 2428–2446.

——, and R. L. Chou, 1994: Parameter sensitivity of the saline circulation. *Climate Dyn.,* **9,** 391–409.

——, and J. Yang, 1996: Deep-water upwelling in the frictional western boundary layer. *J. Phys. Oceanogr.,* **26,** 2243–2250.

Huck, T., 1997: Modeling the large-scale ocean thermohaline circulation: Analysis of its interdecadal variability. Ph.D. thesis, Université de Bretagne Occidentale, Brest, France, 250 pp.

——, A. J. Weaver, and A. Colin de Verdière, 1999: On the influence of the parameterization of lateral boundary layers on the thermohaline circulation in coarse-resolution ocean models. *J. Mar. Res.,* in press.

Jenkins, W. J., 1991: Determination of isopycnal diffusivity in the Sargasso Sea. *J. Phys. Oceanogr.,* **21,** 1058–1061.

Kushnir, Y., 1994: Interdecadal variations in North Atlantic Sea Surface Temperature and associated atmospheric conditions. *J. Climate,* **7,** 141–157.

Ledwell, J. R., A. J. Watson, and C. S. Law, 1993: Evidence for slow

mixing across the pycnocline from an open-ocean tracer-release experiment. *Nature,* **364,** 701–703.
Malkus, W. V. R., 1972: Non-periodic convection at high and low Prandtl number. *Mém. Soc. Roy. Sci. Liège,* **6,** 125–128.
Marotzke, J., 1990: Instabilities and multiple equilibria of the thermohaline circulation. Ph.D. thesis, Institut für Meereskunde, 126 pp.[Available from J. Marotzke at jochem@sound.mit.edu]
——, 1991: Influence of convective adjustment on the stability of the thermohaline circulation. *J. Phys. Oceanogr.,* **21,** 903–907.
——, and D. W. Pierce, 1997: On spatial scales and lifetimes of SST anomalies beneath a diffusive atmosphere. *J. Phys. Oceanogr.,* **27,** 133–139.
Munk, W. H., 1966: Abyssal recipes. *Deep-Sea Res.,* **13,** 707–730.
Ollitrault, M., 1995: La circulation générale de l'Atlantique Nord subtropical vers 700 m de profondeur, révélée par des flotteurs dérivants de subsurface. *C. R. Acad. Sci. Paris,* **321,** 153–160.
Pacanowski, R. C., 1995: MOM 2 documentation, user's guide and reference manual. GFDL Ocean Tech. Rep. 3, 232 pp.
Phillips, N. A., 1963: Geostrophic motion. *Rev. Geophys. Space Phys.,* **1,** 123–176.
Power, S. B., and R. Kleeman, 1994: Surface heat flux parameterizations and the response of ocean general circulation models to high-latitude freshening. *Tellus,* **46A,** 86–95.
Rahmstorf, S., 1993: A fast and complete convection scheme for ocean models. *Ocean Modelling,* **101,** (unpublished manuscript), 9–11.
——, and J. Willebrand, 1995: The role of temperature feedback in stabilizing the thermohaline circulation. *J. Phys. Oceanogr.,* **25,** 787–805.
Reverdin, G., D. Cayan, and Y. Kushnir, 1997: Decadal variability of hydrography in the upper northern North Atlantic in 1948–1990. *J. Geophys. Res.,* **102,** 8505–8531.
Salmon, R., 1986: A simplified linear ocean circulation theory. *J. Mar. Res.,* **44,** 695–711.
——, 1990: The thermocline as an ''internal boundary layer.'' *J. Mar. Res.,* **48,** 437–469.
Saravanan, R., and J. C. McWilliams, 1995: Multiple equilibria, natural variability, and climate transitions in an idealized ocean–atmosphere model. *J. Climate,* **8,** 2296–2323.
Schopf, P. S., 1983: On equatorial waves and El Niño. Part II: Effects of air–sea thermal coupling. *J. Phys. Oceanogr.,* **13,** 1878–1893.
Seager, R., Y. Kushnir, and M. A. Cane, 1995: On heat flux boundary conditions for ocean models. *J. Phys. Oceanogr.,* **25,** 3219–3230.
Stommel, H., 1961: Thermohaline convection with two stable regimes of flow. *Tellus,* **13,** 224–230.
Veronis, G., 1975: The role of models in tracer studies. *Numerical Models of the Ocean Circulation,* 133–146. Natl. Acad. Sci., Washington, DC, 14 pp.
Weaver, A. J., and E. S. Sarachik, 1990: On the importance of vertical resolution in certain OGCM. *J. Phys. Oceanogr.,* **20,** 600–609.
——, and ——, 1991: Evidence for decadal variability in an ocean general circulation model: An advective mechanism. *Atmos.–Ocean,* **29,** 197–231.
——, ——, and J. Marotzke, 1991: Freshwater flux forcing of decadal and interdecadal oceanic variability. *Nature,* **353,** 836–838.
Winton, M., 1993: Numerical investigations of steady and oscillating thermohaline circulations. Ph.D. thesis, University of Washington, 155 pp. [Available from M. Winton at mw@gfdl.gov]
——, 1996: The role of horizontal boundaries in parameter sensitivity and decadal-scale variability of coarse-resolution ocean general circulation models. *J. Phys. Oceanogr.,* **26,** 289–304.
——, 1997: The damping effect of bottom topography on internal decadal-scale oscillations of the thermohaline circulation. *J. Phys. Oceanogr.,* **27,** 203–207.
——, and E. S. Sarachik, 1993: Thermohaline oscillations induced by strong steady salinity forcing of ocean general circulation models. *J. Phys. Oceanogr.,* **23,** 1389–1410.
Yin, F. L., and I. Fung, 1991: Net diffusivity in ocean general circulation models with nonuniform grids. *J. Geophys. Res.,* **96,** 10 773–10 776.
——, and E. Sarachik, 1995: Interdecadal thermohaline oscillations in a sector ocean general circulation model: Advective and convective processes. *J. Phys. Oceanogr.,* **25,** 2465–2484.
Zhang, S., C. A. Lin, and R. J. Greatbatch, 1992: A thermocline model for ocean-climate studies. *J. Mar. Res.,* **50,** 99–124.
——, R. J. Greatbatch, and C. A. Lin, 1993: A reexamination of the polar halocline catastrophe and implications for coupled ocean–atmosphere modeling. *J. Phys. Oceanogr.,* **23,** 287–299.